


Effects of finite volume and magnetic fields on thermodynamic properties of quark matter and fluctuations of conserved charges

Nisha Chahal^{✉,*}, Suneel Dutt,[†] and Arvind Kumar[‡]

Department of Physics, Dr. B R Ambedkar National Institute of Technology Jalandhar, Jalandhar-144011, Punjab, India

 (Received 27 September 2022; revised 20 January 2023; accepted 23 March 2023; published 7 April 2023)

In the current work, we present the influence of finite volume and magnetic field on the thermodynamic properties of isospin asymmetric quark matter using the Polyakov loop extended chiral SU(3) quark mean field (PCQMF) model at finite chemical potential and temperature. Within the PCQMF model, we use the scalar and vector field values in mean-field approximation to obtain the thermodynamic properties: pressure density, entropy density, and energy density. The susceptibilities of conserved charges for strongly interacting matter for different system sizes as well as for different values of the magnetic field have been studied. A sizable shift in phase boundary towards the higher values of quark chemical potential (μ_q) and temperature (T) has been observed for decreasing values of system volume as well as an opposite shift towards lower temperature and quark chemical potential for increasing magnetic field. We observe an enhancement in fluctuations of conserved charges in the regime of the transition temperature. These studies may have a significant role in understanding the thermodynamic observables extracted from heavy-ion collisions data.

DOI: [10.1103/PhysRevC.107.045203](https://doi.org/10.1103/PhysRevC.107.045203)

I. INTRODUCTION

The main aim of heavy-ion collision experiments across the world is to study the phase structure of the strongly interacting matter at extreme conditions of density and temperature [1–3]. Ongoing experimental facilities at the BNL Relativistic Heavy Ion Collider (RHIC) [4,5], the CERN Large Hadron Collider (LHC) [6], as well as upcoming programs like Nuclotron-based Ion Collider facility (NICA) at JINR [7] and Facility for Antiproton and Ion Research (FAIR) [8] at GSI, are aimed at exploring the different regions of quantum chromodynamics (QCD) phase diagram [9].

Alongside the experimental analysis, some hadron properties can also be studied by numerical lattice QCD simulations, which are a nonperturbative application of field theory based on Feynman path integral approach [10,11]. These calculations, performed on various lattice points in a space-time grid have predicted a smooth crossover from confined hadronic state to deconfined quark-gluon plasma phase at high temperatures and low baryonic densities [12,13]. At finite chemical potential values, lattice simulations face the challenge of the fermion sign problem [14–16]. Other theoretical approaches

based on nonperturbative QCD has shown the existence of first-order phase transition at low values of temperature and high baryonic density [17–20]. These two transition regimes are anticipated to be connected by a QCD critical point where the transition is expected to be of the second order [21]. The existence of the critical point, at a temperature value of about 165 MeV and baryonic chemical potential (μ_B) value about 95 MeV, has been suggested by finite-size scaling (FSS) analysis of the data of the beam energy scan (BES) program at RHIC [22]. In order to build upon the results of BES-I, BES Phase-II was launched in 2019 to investigate the phase diagram in intermediate-to-high baryonic chemical potential regimes with high precision [23].

Determination of QCD properties like the equation of state and correlation functions in the neighborhood of a critical point is quite difficult, thus understanding the nature and precise measurement of the location of this point is a matter of ongoing high-priority research both experimentally and theoretically [24]. Many theoretical models and approaches, such as hadron resonance gas (HRG) model [25], Dyson-Schwinger equation framework [26], chiral hadronic model [27], Nambu–Jona-Lasinio (NJL) model [28], Polyakov-quark-meson (PQM) model [29], Polyakov NJL (PNJL) model [30], and functional renormalization group (FRG) [31] approach, have been employed to study the thermodynamic properties of the matter created in heavy-ion collisions.

The influence of nonzero magnetic field on the phase structure of QCD has attracted a great deal of attention as strong magnetic fields are believed to have been produced in the beginning of the universe [32], in magnetars [33] as well as during heavy-ion collisions [34]. Thus it becomes essential to study the phase diagram at finite values of magnetic field

*nishachahal137@gmail.com

†dutts@nitj.ac.in

‡iitd.arvind@gmail.com, kumara@nitj.ac.in

Published by the American Physical Society under the terms of the [Creative Commons Attribution 4.0 International](https://creativecommons.org/licenses/by/4.0/) license. Further distribution of this work must maintain attribution to the author(s) and the published article's title, journal citation, and DOI. Funded by SCOAP³.

along with nonzero chemical potential [35,36]. During the electroweak transition in the early universe, the magnitude of the magnetic field is expected to be as high as eB around $200m_\pi^2$ [37] while the value is estimated to be eB around $0.1 m_\pi^2$ for the CERN Super Proton Synchrotron (SPS) [38], eB of the order of m_π^2 at RHIC [39] and eB approximately $15 m_\pi^2$ at the LHC [40]. In such heavy-ion collisions, charge separation is observed along the orbital momentum axis of the system, also known as the “chiral magnetic effect” due to the strong magnetic fields generated in these collisions [35,41,42]. The influence of external magnetic field on quark matter is determined by analyzing the interaction of valence and sea quarks [43]. In the vicinity of the critical temperature, quark condensate is enhanced due to the valence quarks, but its effect is saturated by sea quarks suppression [44]. Hence we observe a relocation of pseudocritical temperature to lower values with the increase in the magnetic field, termed “inverse magnetic catalysis”. Seemingly contradictory results were obtained in early studies of low energy effective theories and lattice QCD simulations at vanishing values of temperature showing the enhancement of quark condensates, referred as “magnetic catalysis” [45–49]. Magnetic catalysis at zero temperature is attributed to the positive behavior of β function in scalar quantum electrodynamics (QED) [50]. The lattice calculations at more finer grid points and consideration of physical quark masses have also shown the relocation of critical point to a lower temperature value [51]. The effect of the external magnetic field in the PNJL model has been shown to be the catalyzer of dynamical symmetry breaking in quark matter.

In the initial time period after a heavy-ion collision, a finite extent fireball is created, which extends up to the range of a few femtometers in all directions. Also, the possible critical point and its impact is critically blurred out, considering the brief lifetime and small volume of QGP created in heavy-ion collisions [52]. Thus the impact of finite volume on the thermodynamics of matter created after the collision as well as phase transition is quite significant [53,54]. The motivation behind finite volume considerations in studying strong interactions can also be highlighted by FSS analysis [55,56], which is a potent statistical tool working on the idea of comparing the linear dimension L to correlation length, ξ [57]. Theoretical studies have shown the repositioning of critical temperature and chemical potential towards higher values with the decrease in the system volume [58,59]. The impact of finite size has also been studied by considering spherical and cubic regions in the NJL model [60]. Finite size effects have been incorporated in the PNJL model by employing multiple reflection expansion (MRE) formalism [61,62]. This framework describes a sphere rather than a cube and is included in the modification of the density of states [63–65].

Fluctuations and correlations of conserved charges, which are measurable by event-by-event analysis of heavy-ion collisions, carries important information regarding the hot matter created in the collision [66–70]. These have been identified as the observables that can be calculated both experimentally and in theoretical models to have a more precise knowledge of the critical endpoint (CEP). Most importantly, the non-Gaussian

behavior of susceptibilities of conserved charges has recently grabbed much of attention [71]. In lattice QCD, the Polyakov loop susceptibilities in the finite size have been estimated by choosing lattice sizes in the range of palpable volume realized in heavy ion collisions [72]. Using a similar approach, quark number susceptibilities and thermodynamic properties have been investigated by applying Monte Carlo simulations to PNJL model [73]. It has been shown in [74] that with increasing the value of finite size and magnetic field, susceptibilities of conserved quantities have shown significant enhancement of the peaked structure near the transition regime in the QCD phase diagram. The sudden rise in the skewness of the baryon number and strangeness number is highlighted as an essential parameter to explore the QCD critical endpoint [39].

In the present work, we aim to inspect the thermodynamic properties and fluctuations of conserved charges in quark matter, considering the impact of finite volume and finite value of the magnetic field. For this, we have used the formalism of Polyakov loop extended chiral SU(3) quark mean field model [75]. In order to describe a complex many-body problem, we need to consider a relativistic quantum field theory that contains scalar and vector meson fields alongside baryons. In the well-studied phenomenology of a nucleon-nucleon interactions, attractive contribution has been postulated at an intermediate range while the repulsive contribution is populated at a shorter range. These repulsive interactions are modeled in mean-field model by vector mesons, whereas scalar mesons are included to define the attractive interactions [76]. This model comprehends the interaction of quarks by the inclusion of spin-0 and even parity scalar meson fields along with spin-1 and odd parity vector meson fields. The scalar fields are nonstrange scalar field (σ), strange scalar field (ζ), scalar isovector field (δ), and isoscalar dilaton field (χ). The vector fields included in the model are nonstrange vector field (ω), vector-isovector field (ρ), and strange vector field (ϕ). This model has been used in literature to study the properties of finite nuclei [77], hypernuclei [78], and strange hadronic matter [79]. The Polyakov loop potential is included in the chiral SU(3) quark mean field model (CQMF) in order to give a better description of the deconfinement transition and to incorporate the thermal fluctuations arising in the pure gluonic theory [68,80]. With the introduction of the Polyakov loop, theoretical models give a better reproduction of lattice data [81,82]. Quantum and thermal fluctuations of the matter can also be included in theoretical models by using the functional renormalization group (FRG) approach, which is based on flow equations derived from effective action [83,84].

This paper is organized as follows. In Sec. II A, we have briefly described the PCQMF and have obtained the grand canonical potential and thermodynamic quantities. In Sec. II B, Taylor series method is discussed in detail for the description of cumulants and hence susceptibilities. In Sec. III, a descriptive view of all the results for thermodynamic properties of quark matter, a phase diagram of QCD for finite volume and magnetic field and fluctuations has been presented. In Sec. IV, we have summarized the results of the present work.

II. METHODOLOGY

A. Polyakov chiral SU(3) quark mean field model

The CQMF model incorporates the meson-meson and quark-meson interactions and is based on chiral $SU(3)_L \times SU(3)_R$ symmetry, it is spontaneous breaking [85,86], and also the broken scale invariance [87]. In this model, quarks are bound in the hadrons by an effective mean field potential and are used to explain many-body interactions based on a relativistic nonperturbative approach. The masses of pseudoscalar mesons are derived from explicit symmetry breaking, while the masses of quarks and other mesons are attributed to the spontaneous symmetry breaking [88]. The total effective Lagrangian density of the model in order to study strange quark matter is written as [89]

$$\mathcal{L}_{\text{eff}} = \mathcal{L}_{q0} + \mathcal{L}_{qm} + \mathcal{L}_{\Sigma\Sigma} + \mathcal{L}_{VV} + \mathcal{L}_{SB} + \mathcal{L}_{\Delta m} + \mathcal{L}_h, \quad (1)$$

where $\mathcal{L}_{q0} = \bar{q} i\gamma^\mu \partial_\mu q$ gives the free part of massless quarks. The quark meson interaction term, \mathcal{L}_{qm} splits into right- and left-handed parts in chiral limits and is represented as [68]

$$\begin{aligned} \mathcal{L}_{qm} = & g_s (\bar{\psi}_L M \psi_R + \bar{\psi}_R M^\dagger \psi_L) \\ & - g_v (\bar{\psi}_L \gamma^\mu l_\mu \psi_L + \bar{\psi}_R \gamma^\mu r_\mu \psi_R). \end{aligned} \quad (2)$$

In the above equation, the quark spinor, $\psi = (u, d, s)$ for $N_c = 3$, color degrees of freedom, g_v and g_s define the coupling strength of vector and scalar mesons with quarks, respectively. The nonets for spin-zero and -one mesons can be written as

$$M(M^\dagger) = \Sigma \pm i\Pi = \frac{1}{\sqrt{2}} \sum_{a=0}^8 (\sigma^a \pm i\pi^a) \lambda^a \quad (3)$$

and

$$l_\mu(r_\mu) = \frac{1}{2}(V_\mu \pm A_\mu) = \frac{1}{2\sqrt{2}} \sum_{a=0}^8 (v_\mu^a \pm a_\mu^a) \lambda^a. \quad (4)$$

In Eq. (3), Σ and Π represent the spin-0 scalar and pseudoscalar mesons. Nonets of vector and pseudovector mesons are given by v_μ^a and a_μ^a , respectively. The third and the fourth term in Eq. (1) expresses the self-interactions of scalar mesons and vector mesons, respectively. The attractive contribution of interactions in the medium is attributed by the inclusion of scalar mesons. These self-interaction terms of mesons are given as

$$\begin{aligned} \mathcal{L}_{\Sigma\Sigma} = & -\frac{1}{2} k_0 \chi^2 (\sigma^2 + \zeta^2 + \delta^2) + k_1 (\sigma^2 + \zeta^2 + \delta^2)^2 \\ & + k_2 \left(\frac{\sigma^4}{2} + \frac{\delta^4}{2} + 3\sigma^2 \delta^2 + \zeta^4 \right) \\ & + k_3 \chi (\sigma^2 - \delta^2) \zeta - k_4 \chi^4 - \frac{1}{4} \chi^4 \ln \frac{\chi^4}{\chi_0^4} \\ & + \frac{d}{3} \chi^4 \ln \left(\left(\frac{(\sigma^2 - \delta^2) \zeta}{\sigma_0^2 \zeta_0} \right) \left(\frac{\chi^3}{\chi_0^3} \right) \right), \end{aligned} \quad (5)$$

$$\begin{aligned} \mathcal{L}_{VV} = & \frac{1}{2} \frac{\chi^2}{\chi_0^2} (m_\omega^2 \omega^2 + m_\rho^2 \rho^2 + m_\phi^2 \phi^2) \\ & + g_4 (\omega^4 + 6\omega^2 \rho^2 + \rho^4 + 2\phi^4). \end{aligned} \quad (6)$$

The interaction of mesons with quarks is described by the interchange of scalar as well as vector meson fields. In order to study strange matter, it is quite important to include a strange scalar isoscalar field, ζ , due to its strange quark content. The scalar isovector field, δ , gives the description of isospin asymmetric matter. In reality, chiral SU(3) symmetry is not satisfied exactly by quark-meson interactions. This is due to the fact that pseudoscalar mesons are Goldstone bosons with zero mass, but the masses of K and π mesons are not zero. Hence, the contribution of explicit symmetry breaking in the effective Lagrangian is included by \mathcal{L}_{SB} , $\mathcal{L}_{\Delta m}$, and \mathcal{L}_h [77,90]. The term \mathcal{L}_{SB} gives rise to nonzero masses for pseudoscalar mesons and is given by

$$\mathcal{L}_{SB} = -\frac{\chi^2}{\chi_0^2} \left[m_\pi^2 f_\pi \sigma + \left(\sqrt{2} m_K^2 f_K - \frac{m_\pi^2}{\sqrt{2}} f_\pi \right) \zeta \right]. \quad (7)$$

The partially conserved axial-vector current (PCAC) relations are thus satisfied for K and π mesons as a result of nonvanishing divergence of axial currents. An additional mass term is included in the model, which gives the reasonable constituent mass of strange quark, represented as

$$\mathcal{L}_{\Delta m} = -\Delta m_s \bar{q} S q, \quad (8)$$

where $S = \frac{1}{3}(I - \lambda_8 \sqrt{3})$ is the strangeness quark matrix. The term $\mathcal{L}_h = (h_1 \sigma + h_2 \zeta) \bar{s} s$, describes hyperon potential in the mean-field approximation.

For good reproduction of lattice data, effective chiral models are extended by the introduction of different forms of Polyakov-loop potential. Due to the success of this approach, effective models can be seen as an enticing method to study strange hadronic and quark matter. Hence it becomes possible to study both chiral symmetry breaking and deconfinement in the upgraded model. Thus the total Lagrangian of the PCQMF model is defined as

$$\mathcal{L}_{\text{PCQMF}} = \mathcal{L}_{\text{eff}} - \mathcal{U}(\Phi(\vec{x}), \bar{\Phi}(\vec{x}), T), \quad (9)$$

where $\mathcal{U}(\Phi(\vec{x}), \bar{\Phi}(\vec{x}), T)$ is the effective Polyakov loop potential. In the above equation, Φ and $\bar{\Phi}$ are the Polyakov-loop variables and are defined as the expectation value of trace over the color of the thermal Wilson line [89]. Polyakov loop potential is not uniquely defined and can be constructed from the center symmetry of the pure-gauge theory. For this work, we consider the polynomial parameterized form of Polyakov loop potential, which is given by [91,92]

$$\frac{\mathcal{U}_{\text{poly}}(\Phi, \bar{\Phi})}{T^4} = -\frac{b_2(T)}{2} \bar{\Phi} \Phi - \frac{b_3}{6} (\Phi^3 + \bar{\Phi}^3) + \frac{b_4}{4} (\bar{\Phi} \Phi)^2. \quad (10)$$

The temperature-dependent coefficient, $b_2(T)$, appearing in the above equation, is defined as

$$b_2(T) = a_0 + a_1 \left(\frac{T_0}{T} \right) + a_2 \left(\frac{T_0}{T} \right)^2 + a_3 \left(\frac{T_0}{T} \right)^3. \quad (11)$$

The parameters are determined by fitting the lattice simulation data and hence we consider the following: $a_0 = 1.53$, $a_1 = 0.96$, $a_2 = -2.3$, $a_3 = -2.85$, $b_3 = 13.34$, and $b_4 = 14.88$. Here, T_0 is the critical temperature for the change of phase

from confined hadrons to deconfined quarks in the pure Yang-Mills theory at a very low value of chemical potential [93]. Thus the thermodynamic potential for the PCQMF model is defined as

$$\Omega = \mathcal{U}(\Phi, \bar{\Phi}, T) + \Omega_{q\bar{q}} - \mathcal{L}_M - \mathcal{V}_{vac}. \quad (12)$$

In the above equation, $\mathcal{L}_M = \mathcal{L}_{VV} + \mathcal{L}_{\Sigma\Sigma} + \mathcal{L}_{SB}$, is the meson interaction term. The vacuum term, \mathcal{V}_{vac} is subtracted in order to obtain zero vacuum energy. The thermal contribution of quarks and antiquarks to the total thermodynamic potential is represented by

$$\Omega_{q\bar{q}} = - \sum_{i=u,d,s} \gamma_i T \int_0^\infty \frac{d^3 p}{(2\pi)^3} [\ln(g_i^+) + \ln(g_i^-)]. \quad (13)$$

In the above equation, g_i^+ and g_i^- are defined as

$$g_i^+ = [1 + 3\Phi e^{-(E_i^* - v_i^*)/T} + 3\bar{\Phi} e^{-2(E_i^* - v_i^*)/T} + e^{-3(E_i^* - v_i^*)/T}] \quad (14)$$

and

$$g_i^- = [1 + 3\bar{\Phi} e^{-(E_i^* + v_i^*)/T} + 3\Phi e^{-2(E_i^* + v_i^*)/T} + e^{-3(E_i^* + v_i^*)/T}]. \quad (15)$$

Here, the summation is over the constituent quarks, and γ_i is the spin degeneracy factor. In the above equation, $v_i^* = \mu_i - g_{\omega i} \omega - g_{\phi i} \phi - g_{\rho i} \rho$ is the effective chemical potential derived from vector fields. The effective single particle energy is calculated in terms of the effective constituent mass of quarks, $m_i^* = -g_{\sigma i} \sigma - g_{\zeta i} \zeta - g_{\delta i} \delta + m_{i0}$, where $m_{u0} = m_{d0} = 0$ and $m_{s0} = 29$ MeV. The $g_{\sigma i}$, $g_{\zeta i}$, $g_{\delta i}$ give the coupling strength of different quarks with scalar mesons and $g_{\omega i}$, $g_{\rho i}$, $g_{\phi i}$ for vector mesons. The effective energy of quarks is defined as

$$E_i^* = \sqrt{p^2 + m_i^{*2}}. \quad (16)$$

Now, in order to study the impact of magnetic field on the strange quark matter in PCQMF model, we consider a homogeneous magnetic field, B in the z direction. In the presence of the finite magnetic field, the total effective energy of the quarks is modified as [94,95]

$$E_i^* = \sqrt{p_z^2 + m_i^{*2} + |q_i|(2n + 1 - \Upsilon)B} \quad (17)$$

and

$$p = \sqrt{p_z^2 + |q_i|(2n + 1 - \Upsilon)B}. \quad (18)$$

The above equation gives the relation of total momentum, p with the longitudinal momentum, p_z and Υ defines the spin quantum number $S(\Upsilon = \pm S/2)$. Now, $2n + 1 - \Upsilon$ can be replaced by a single quantum number, k , known as the Landau level. Thus the total thermodynamical potential is altered, and the term giving the contribution of quarks and antiquarks interaction is written as [39,59]

$$\Omega_{q\bar{q}} = - \sum_{i=u,d,s} \frac{|q_i|BT}{2\pi} \sum_{k=0}^{\infty} \alpha_k \int_{-\infty}^{\infty} \frac{dp_z}{2\pi} (\ln g_i^+ + \ln g_i^-). \quad (19)$$

The summation in Eq. (19) runs over the lowest Landau level, $k = 0$ to the maximum occupied Landau level [96]. Here, α_k is the spin-degeneracy factor and due to the polarization of charged particles in the lowest Landau levels by the external magnetic field, its value is 1 for $k = 0$ and 2 otherwise. The impact of the finite size effect is assimilated in the model by using the approximation method defined in [58,97,98] by introducing a lower momentum cutoff, p_{\min} [MeV] = π/R [MeV] = Λ , where R is the length of a cubic volume. In order to consider the complete execution of finite volume, one has to carefully analyze the impact of the surface and curvature of the system under examination. Along with this, periodic boundary conditions for bosons and antiperiodic conditions for fermions have to be scrutinized, leading to the indeterminable sum over discrete momentum values [58]. In NJL and PNJL models, the fermion vacuum term is accountable for dynamical chiral symmetry breaking in the vacuum and is thus considered with proper divergence regularization of a ultraviolet cutoff parameter [99]. On the contrary, spontaneous breaking of chiral symmetry is incorporated through the mesonic potential in the current model, as in PQM and PLSM models [29,100]. Due to the inclusion of the fermion vacuum term in the PQM model, the critical temperature has been reported to shift towards the higher values of baryonic chemical potential and low values of temperature [101,102]. The fermion vacuum term has not been considered in the current work and hence, no upper cutoff on momentum has been implied.

In order to calculate the values of different fields at the varying value of temperatures and density, we minimize the total thermodynamic potential obtained after the inclusion of external magnetic field and finite volume. Thus we have

$$\frac{\partial \Omega}{\partial \sigma} = \frac{\partial \Omega}{\partial \zeta} = \frac{\partial \Omega}{\partial \delta} = \frac{\partial \Omega}{\partial \chi} = \frac{\partial \Omega}{\partial \omega} = \frac{\partial \Omega}{\partial \rho} = \frac{\partial \Omega}{\partial \phi} = \frac{\partial \Omega}{\partial \Phi} = \frac{\partial \Omega}{\partial \bar{\Phi}} = 0. \quad (20)$$

Plugging Ω in above, the following system of equations is obtained:

$$\begin{aligned} \frac{\partial \Omega}{\partial \sigma} &= k_0 \chi^2 \sigma - 4k_1 (\sigma^2 + \zeta^2 + \delta^2) \sigma - 2k_2 (\sigma^3 + 3\sigma \delta^2) - 2k_3 \chi \sigma \zeta \\ &- \frac{d}{3} \chi^4 \left(\frac{2\sigma}{\sigma^2 - \delta^2} \right) + \left(\frac{\chi}{\chi_0} \right)^2 m_\pi^2 f_\pi - \left(\frac{\chi}{\chi_0} \right)^2 m_\omega \omega^2 \frac{\partial m_\omega}{\partial \sigma} - \left(\frac{\chi}{\chi_0} \right)^2 m_\rho \rho^2 \frac{\partial m_\rho}{\partial \sigma} - \sum_{i=u,d} g_{\sigma i} \rho_{si} = 0, \end{aligned} \quad (21)$$

$$\frac{\partial \Omega}{\partial \zeta} = k_0 \chi^2 \zeta - 4k_1(\sigma^2 + \zeta^2 + \delta^2)\zeta - 4k_2 \zeta^3 - k_3 \chi(\sigma^2 - \delta^2) - \frac{d}{3} \frac{\chi^4}{\zeta} + \left(\frac{\chi}{\chi_0}\right)^2 \left[\sqrt{2} m_K^2 f_K - \frac{1}{\sqrt{2}} m_\pi^2 f_\pi \right] - \left(\frac{\chi}{\chi_0}\right)^2 m_\phi \phi^2 \frac{\partial m_\phi}{\partial \zeta} - \sum_{i=s} g_{\zeta i} \rho_{si} = 0, \quad (22)$$

$$\frac{\partial \Omega}{\partial \delta} = k_0 \chi^2 \delta - 4k_1(\sigma^2 + \zeta^2 + \delta^2)\delta - 2k_2(\delta^3 + 3\sigma^2 \delta) + 2k_3 \chi \delta \zeta + \frac{2}{3} d \chi^4 \left(\frac{\delta}{\sigma^2 - \delta^2} \right) - \sum_{i=u,d} g_{\delta i} \rho_{si} = 0, \quad (23)$$

$$\frac{\partial \Omega}{\partial \chi} = k_0 \chi(\sigma^2 + \zeta^2 + \delta^2) - k_3(\sigma^2 - \delta^2)\zeta + \chi^3 \left[1 + \ln \left(\frac{\chi^4}{\chi_0^4} \right) \right] + (4k_4 - d)\chi^3 - \frac{4}{3} d \chi^3 \ln \left(\left(\frac{(\sigma^2 - \delta^2)\zeta}{\sigma_0^2 \zeta_0} \right) \left(\frac{\chi}{\chi_0} \right)^3 \right) + \frac{2\chi}{\chi_0^2} \left[m_\pi^2 f_\pi \sigma + \left(\sqrt{2} m_K^2 f_K - \frac{1}{\sqrt{2}} m_\pi^2 f_\pi \right) \zeta \right] - \frac{\chi}{\chi_0^2} (m_\omega^2 \omega^2 + m_\rho^2 \rho^2) = 0, \quad (24)$$

$$\frac{\partial \Omega}{\partial \omega} = \frac{\chi^2}{\chi_0^2} m_\omega^2 \omega + 4g_4 \omega^3 + 12g_4 \omega \rho^2 - \sum_{i=u,d} g_{\omega i} \rho_{vi} = 0, \quad (25)$$

$$\frac{\partial \Omega}{\partial \rho} = \frac{\chi^2}{\chi_0^2} m_\rho^2 \rho + 4g_4 \rho^3 + 12g_4 \omega^2 \rho - \sum_{i=u,d} g_{\rho i} \rho_{vi} = 0, \quad (26)$$

$$\frac{\partial \Omega}{\partial \phi} = \frac{\chi^2}{\chi_0^2} m_\phi^2 \phi + 8g_4 \phi^3 - \sum_{i=s} g_{\phi i} \rho_{vi} = 0, \quad (27)$$

$$\frac{\partial \Omega}{\partial \Phi} = \left[\frac{-a(T)\bar{\Phi}}{2} - \frac{6b(T)(\bar{\Phi} - 2\Phi^2 + \bar{\Phi}^2\Phi)}{1 - 6\bar{\Phi}\Phi + 4(\bar{\Phi}^3 + \Phi^3) - 3(\bar{\Phi}\Phi)^2} \right] T^4 - \sum_{i=u,d,s} \frac{2TN_C}{(2\pi)^3} \int_0^\infty d^3k \left[\frac{e^{-(E_i^* - v_i^*)/T}}{g_i^+} + \frac{e^{-2(E_i^* + v_i^*)/T}}{g_i^-} \right] = 0, \quad (28)$$

and

$$\frac{\partial \Omega}{\partial \bar{\Phi}} = \left[\frac{-a(T)\Phi}{2} - \frac{6b(T)(\Phi - 2\bar{\Phi}^2 + \Phi^2\bar{\Phi})}{1 - 6\bar{\Phi}\Phi + 4(\bar{\Phi}^3 + \Phi^3) - 3(\bar{\Phi}\Phi)^2} \right] T^4 - \sum_{i=u,d,s} \frac{2TN_C}{(2\pi)^3} \int_0^\infty d^3k \left[\frac{e^{-2(E_i^* - v_i^*)/T}}{g_i^+} + \frac{e^{-(E_i^* + v_i^*)/T}}{g_i^-} \right] = 0. \quad (29)$$

The coupling constants $g_{\sigma i}$, $g_{\zeta i}$, and m_{s0} are calculated by fitting the vacuum masses of constituent quarks as $m_u = m_d = 313$ MeV and $m_s = 490$ MeV. The free model parameters $h_1, h_2, k_0, k_1, k_2, k_3, k_4, g_s$, and g_v are calculated by considering the vacuum masses of σ, ζ , and χ meson along with the masses of K and π mesons and mean masses of η and η' mesons which are expressed by the eigenvalues of the mass matrix [103]. The relations between various quark meson coupling constants is given as

$$\frac{g_s}{\sqrt{2}} = g_\sigma^u = g_\sigma^d = \frac{1}{\sqrt{2}} g_\zeta^s = g_\delta^u = -g_\delta^d, \quad g_\sigma^s = g_\zeta^u = g_\zeta^d = g_\delta^s = 0, \quad (30)$$

$$\frac{g_v}{2\sqrt{2}} = g_\omega^u = g_\omega^d = g_\rho^u = -g_\rho^d = \frac{1}{\sqrt{2}} g_\phi^s, \quad g_\omega^s = g_\rho^s = g_\phi^u = g_\phi^d = 0. \quad (31)$$

The flavor asymmetry is assimilated in the model by including isospin (μ_I) and strangeness chemical potential, μ_S . The baryon, strangeness, and isospin chemical potential are determined through relations

$$\begin{aligned} \mu_B &= \frac{3}{2}(\mu_u + \mu_d), \\ \mu_S &= \frac{1}{2}(\mu_u + \mu_d - 2\mu_s), \\ \mu_I &= \frac{1}{2}(\mu_u - \mu_d). \end{aligned} \quad (32)$$

The vector and scalar density of quarks are defined as

$$\rho_{vi} = \sum_{i=u,d,s} \frac{N_c |q_i| B}{2\pi} \sum_{k=0}^\infty \alpha_k \int_{-\infty}^\infty \frac{dp_z}{2\pi} (f_i - \bar{f}_i) \quad (33)$$

and

$$\rho_{si} = \sum_{i=u,d,s} \frac{N_c |q_i| B}{2\pi} \sum_{k=0}^\infty \alpha_k \int_{-\infty}^\infty \frac{dp_z}{2\pi} \frac{m_i^*}{E_i^*(k)} (f_i + \bar{f}_i). \quad (34)$$

In the above equations, f_i and \bar{f}_i are the Fermi distribution functions at the finite value of temperature for quarks and antiquarks and are defined as

$$f_i = \frac{\Phi e^{-(E_i^* - v_i^*)/T} + 2\bar{\Phi} e^{-2(E_i^* - v_i^*)/T} + e^{-3(E_i^* - v_i^*)/T}}{g_i^+}, \quad (35)$$

$$\bar{f}_i = \frac{\bar{\Phi} e^{-(E_i^* + v_i^*)/T} + 2\Phi e^{-2(E_i^* + v_i^*)/T} + e^{-3(E_i^* + v_i^*)/T}}{g_i^-}. \quad (36)$$

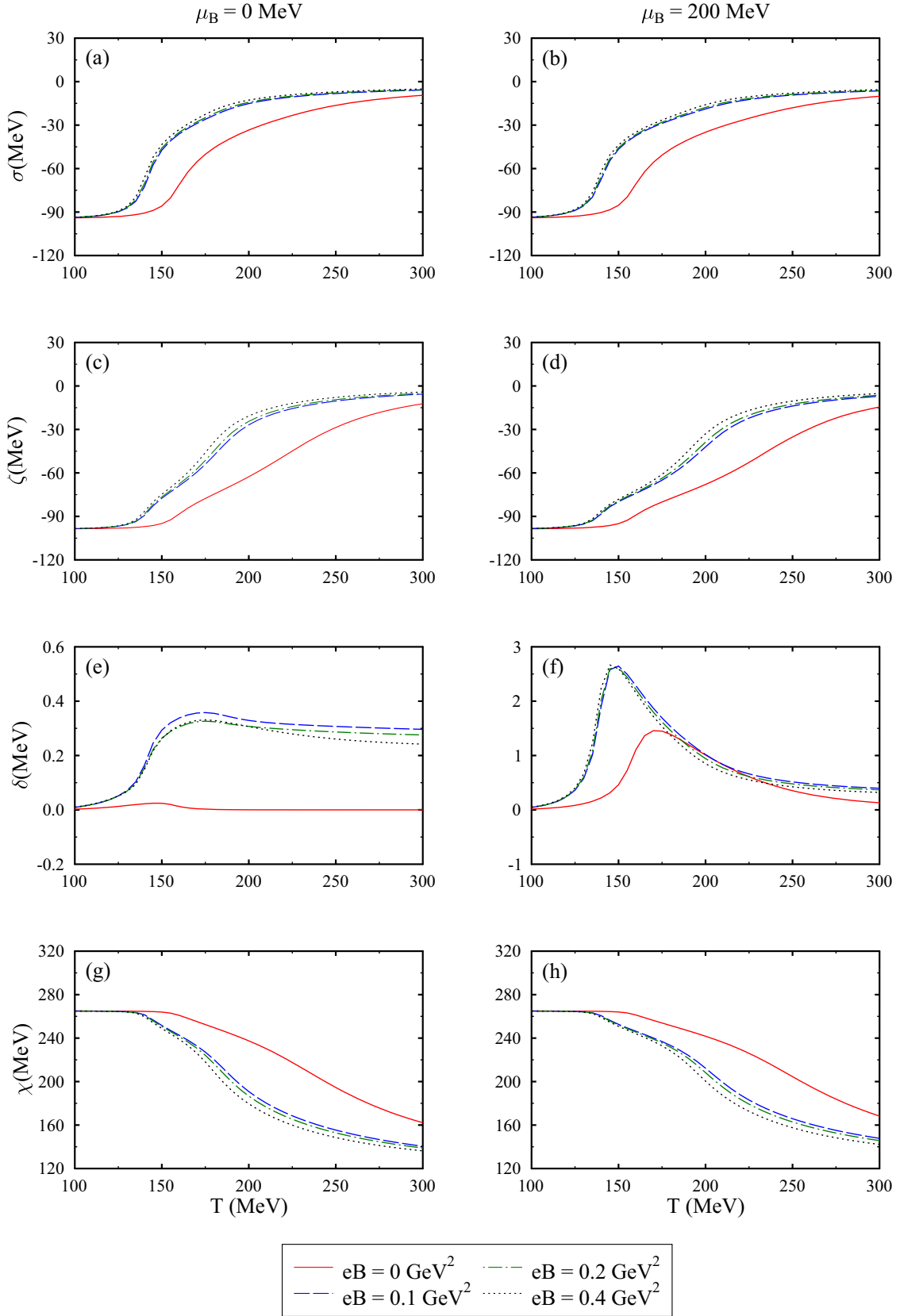


FIG. 1. The scalar fields σ , ζ , δ , and χ are shown as a function of temperature T , for magnetic field $eB = 0, 0.1, 0.2$, and 0.4 GeV^2 and length of cubic volume $R = \infty$, baryonic chemical potential $\mu_B = 0$ and 200 MeV , isospin chemical potential $\mu_I = 80 \text{ MeV}$, and strangeness chemical potential $\mu_S = 200 \text{ MeV}$.

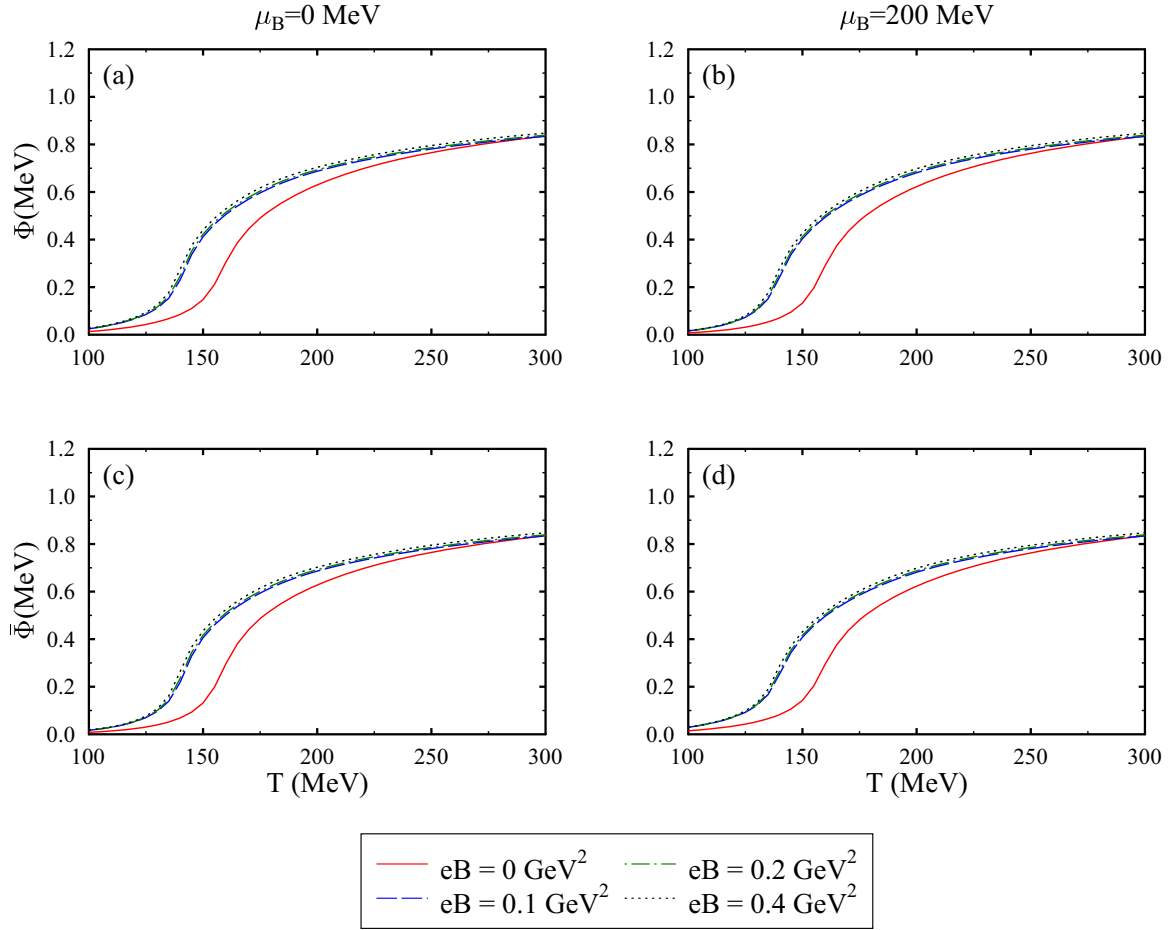


FIG. 2. The Polyakov loop fields, Φ and $\bar{\Phi}$ shown as a function of temperature T , for magnetic field $eB = 0, 0.1, 0.2,$ and 0.4 GeV^2 and length of cubic volume $R = \infty$, baryonic chemical potential $\mu_B = 0$ and 200 MeV , isospin chemical potential $\mu_I = 80 \text{ MeV}$, and strangeness chemical potential $\mu_S = 200 \text{ MeV}$.

B. Thermodynamic quantities and Taylor series expansion

After the calculation of σ , ζ , and δ , the dilaton field χ , the vector fields ω , ρ , and ϕ and the Polyakov fields Φ and its conjugate $\bar{\Phi}$, the thermodynamic potential density is used to calculate the pressure p , entropy density s , and the energy density ϵ , given by

$$p = -\Omega, \quad (37)$$

$$s = -\frac{\partial \Omega}{\partial T}, \quad (38)$$

and

$$\epsilon = \Omega + \sum_{i=u,d,s} v_i^* \rho_i + TS. \quad (39)$$

By substituting the value of pressure derived from the above equation, we can write a generalized expression for the susceptibilities of conserved charges as [104]

$$\chi_{ijk}^{BQS} = \frac{\partial^{i+j+k} [P/T^4]}{\partial (\mu_B/T)^i \partial (\mu_Q/T)^j \partial (\mu_S/T)^k}. \quad (40)$$

Here, μ_B is the baryon chemical potential, μ_Q is the charge number chemical potential, and μ_S stands for the strangeness chemical potential. In heavy ion collision experiments, the susceptibilities of conserved charges in Eq. (40) are also correlated to the cumulants of conserved charge multiplicity distributions. The susceptibilities and correlations are hence computed in terms of the ensemble average of these conserved quantities, $\delta N_X = N_X - \langle N_X \rangle$ [71,105].

In order to have a better understanding of the experimentally derived observables, these fluctuations can be evaluated theoretically by different methods. In [106], the net quark number density fluctuations and higher-order cumulants have been investigated by using FRG approach in Polyakov quark meson model. Baryon and quark number fluctuations have also been calculated by the Dyson-Schwinger equation approach in [107,108]. We use Taylor series expansion in the current work to compute the susceptibilities of conserved charges [109,110]. The scaled pressure in equation 40 is expanded for $\mu_{(B,Q,S)} = 0$ as

$$\frac{P(T, \mu_{(B,Q,S)})}{T^4} = \sum_{n=0}^{\infty} c_n(T) \left(\frac{\mu_{(B,Q,S)}}{T} \right)^n. \quad (41)$$

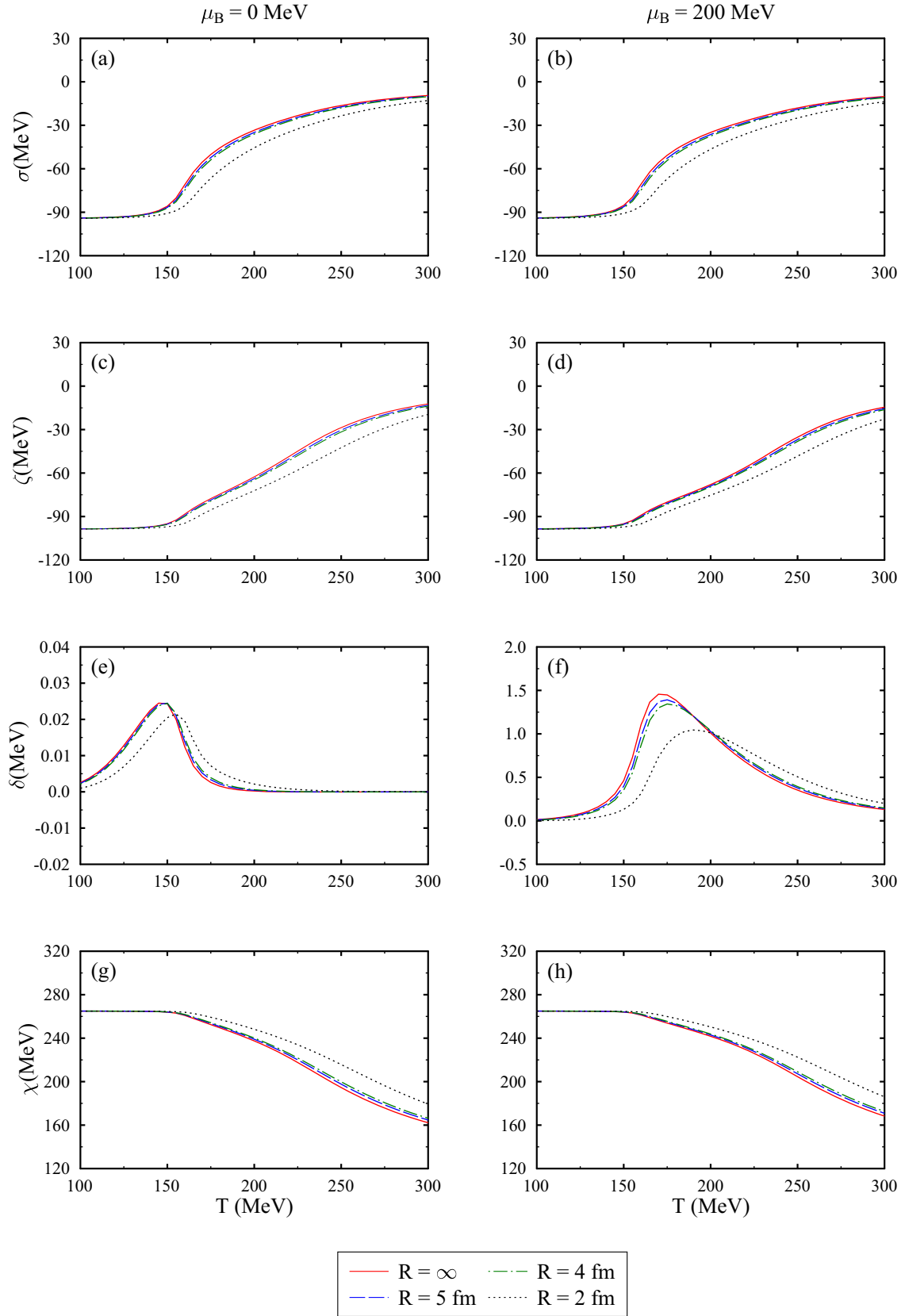


FIG. 3. The scalar fields σ , ζ , δ , and χ shown as a function of temperature T , for length of cubic volume $R = \infty, 5, 4$, and 2 fm and magnetic field $eB = 0$, baryonic chemical potential $\mu_B = 0$ and 200 MeV, isospin chemical potential $\mu_I = 80$ MeV, and strangeness chemical potential $\mu_S = 200$ MeV.

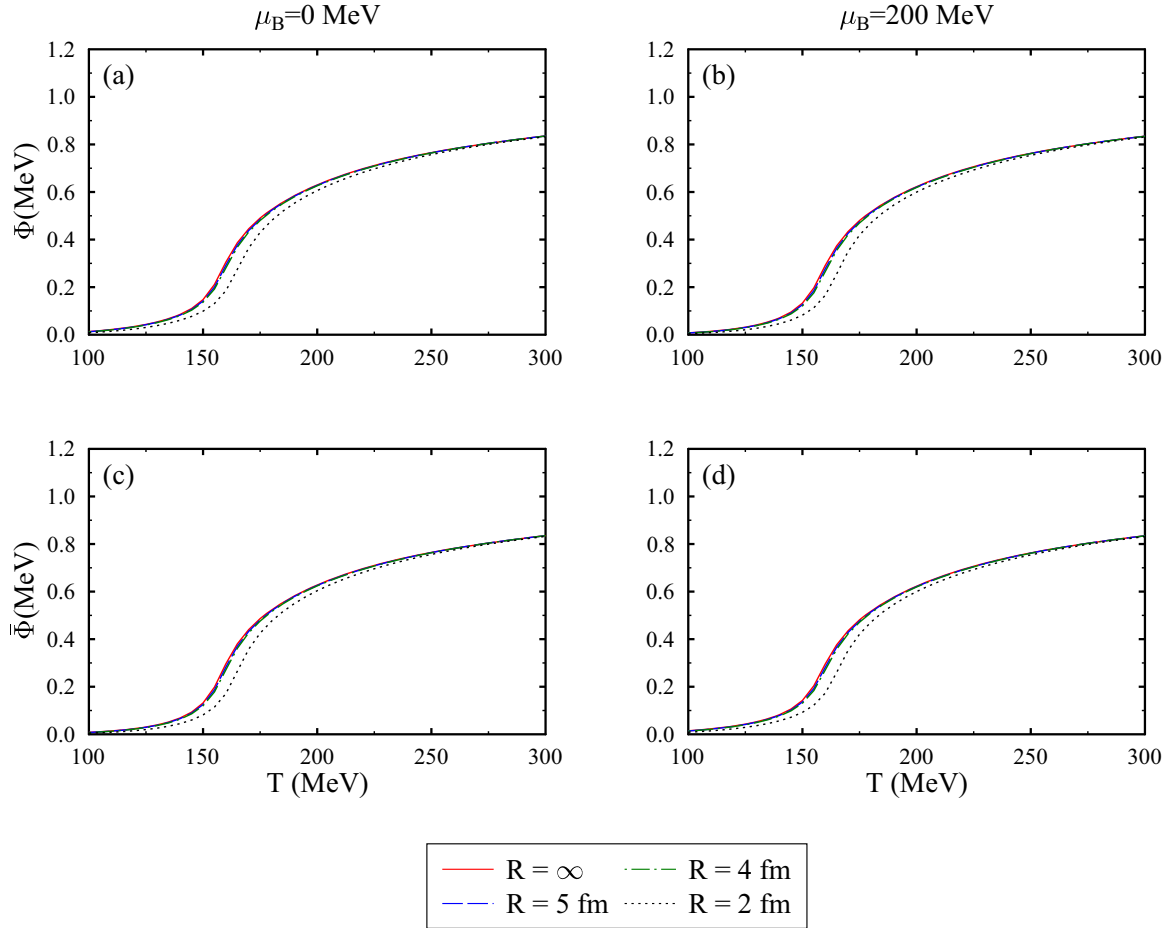


FIG. 4. The Polyakov loop fields, Φ and $\bar{\Phi}$ shown as a function of temperature T , for length of cubic volume, $R = \infty, 5, 4,$ and 2 fm and magnetic field $eB = 0$, baryonic chemical potential $\mu_B = 0$ and 200 MeV, isospin chemical potential $\mu_I = 80$ MeV, and strangeness chemical potential, $\mu_S = 200$ MeV.

So the coefficients of the above series, give the derivatives of conserved charges at vanishing value of chemical potential and thus the susceptibilities.

III. RESULTS AND DISCUSSION

In this section, we present the results for different thermodynamic properties of isospin asymmetric quark matter due to the inclusion of finite volume and magnetic field in the Polyakov loop extended chiral SU(3) quark mean-field model. The values of different fields at varying temperature and density values are obtained by solving the nonlinear coupled equations mentioned earlier. The parameters used in the current study are listed in Tables I and II. In Sec. III A, we

TABLE I. The list of constant values used to fit the model's parameters.

σ_0 (MeV)	ζ_0 (MeV)	χ_0 (MeV)	m_π (MeV)	f_π (MeV)	m_K (MeV)
-93	-96.87	254.6	139	93	496
f_K (MeV)	m_ω (MeV)	m_ϕ (MeV)	m_ρ (MeV)	ρ_0 (fm $^{-3}$)	
115	783	1020	783	0.15	

discuss the in-medium behavior of scalar and vector fields and the Polyakov loop field in the presence of a finite magnetic field and finite volume. Additionally, in-medium masses of quarks and various thermodynamic quantities have also been studied. In Sec. III B, we discuss in detail the impact of finite size and magnetic field on the susceptibilities of conserved charges.

A. Thermodynamic properties and phase diagram

In this section, we have highlighted the impact of the predefined length of cubic volume, and external magnetic

TABLE II. The list of fitted parameters used in the current work.

k_0	k_1	k_2	k_3	k_4	g_s	g_v	g_4
4.94	2.12	-10.16	-5.38	-0.06	4.76	1.95	37.5
d	$g_{\zeta d}$	$g_{\zeta s}$	$g_{\delta u}$	$g_{\delta d}$	$g_{\delta s}$	$g_{\omega u}$	$g_{\omega d}$
0.18	0	4.76	3.36	-3.36	0	0.336	0.336
$g_{\omega s}$	$g_{\phi u}$	$g_{\phi d}$	$g_{\phi s}$	$g_{\rho u}$	$g_{\rho d}$	$g_{\rho s}$	h_1
0	0	0	0.975	0.336	-0.336	0	-2.20
h_2	$g_{\sigma u}$	$g_{\sigma d}$	$g_{\sigma s}$	$g_{\zeta u}$			
3.24	3.36	3.36	0	0			

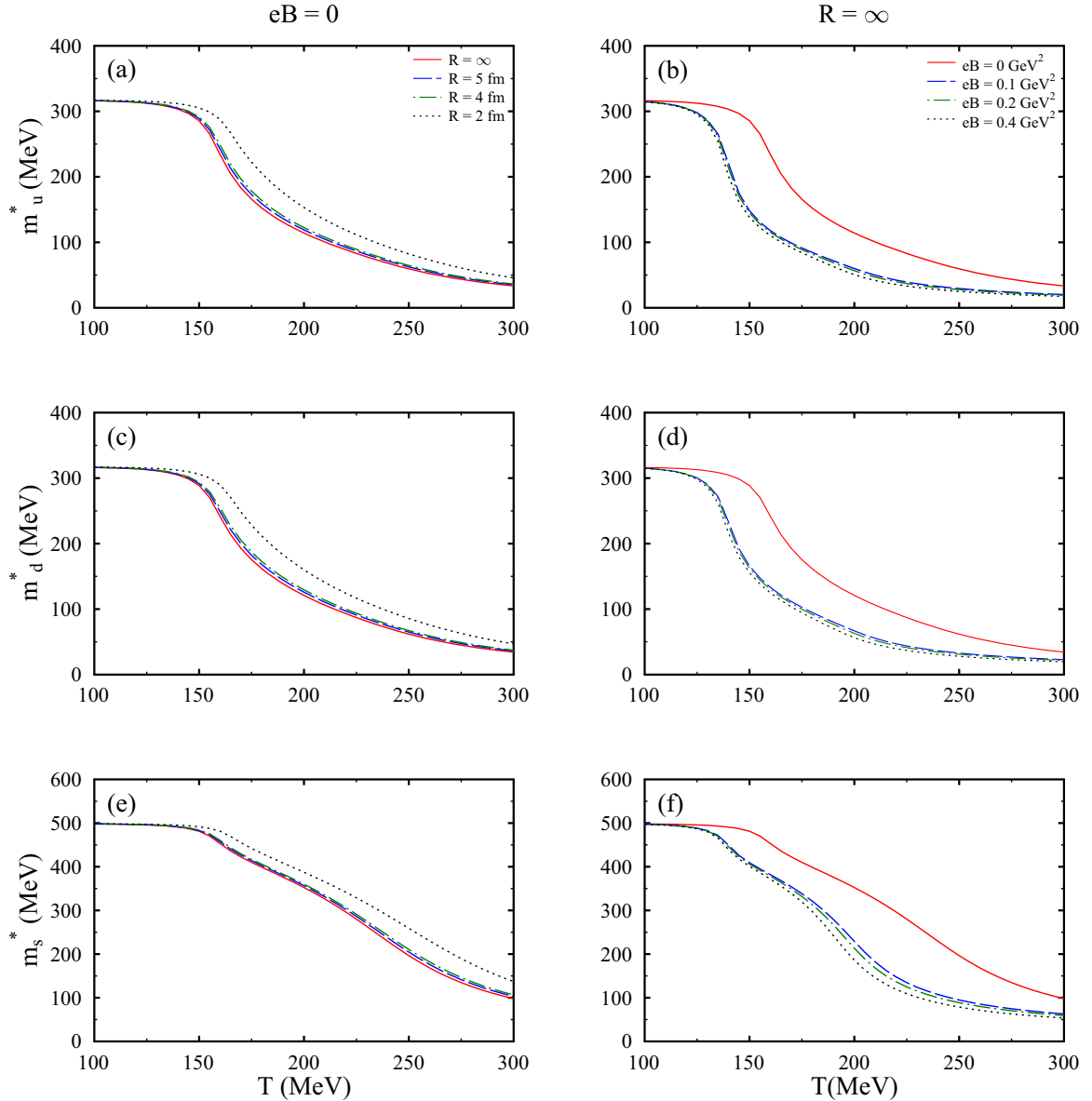


FIG. 5. The effective quark masses m_u^* , m_d^* , and m_s^* shown as a function of temperature T , for different values of length of cubic volume (R) and magnetic field (eB), baryonic chemical potential fixed at $\mu_B = 200$ MeV, isospin chemical potential $\mu_I = 80$ MeV, and strangeness chemical potential $\mu_S = 200$ MeV.

field on the chiral and deconfinement phase transitions of the Polyakov loop extended chiral quark mean field model. The asymmetry of the medium is assimilated by the induction of isospin chemical potential $\mu_I = 80$ MeV, and strangeness chemical potential μ_S is fixed at 200 MeV from Figs. 1–6. In Figs. 1 and 2, we have shown the variation of σ , ζ , δ , χ fields and Polyakov loop fields Φ and $\bar{\Phi}$ as a function of temperature T for baryonic chemical potential $\mu_B = 0$ and 200 MeV and magnetic field $eB = 0, 0.1, 0.2$, and 0.4 GeV². We have noticed that for a given value of μ_B , the value of the σ and ζ fields is constant till a specific temperature value is reached, after which the magnitude starts decreasing with the further increase in the temperature. The temperature at which we observe a sudden fall in the magnitude of scalar fields,

is termed as pseudocritical temperature T_p and is determined from the inflection points of the scalar fields. For the scalar field σ one inflection point is observed whereas for ζ field two points are found. As we will see later, the position of inflection points will be determined from the derivatives of these scalar fields as a function of temperature. With the increase in the magnitude of the magnetic field for a given value of μ_B and T , we observe a drop in the magnitude of σ , ζ , and χ field. As discussed in Sec. I, this slackening due to the external magnetic field is accredited to the suppression of quark condensate, referred as “inverse magnetic catalysis”.

At finite and zero values of μ_B , it is clear that the value of T_p is shifted to a lower temperature value. The magnitude of σ , ζ , δ , and χ fields increases with the increase in baryonic

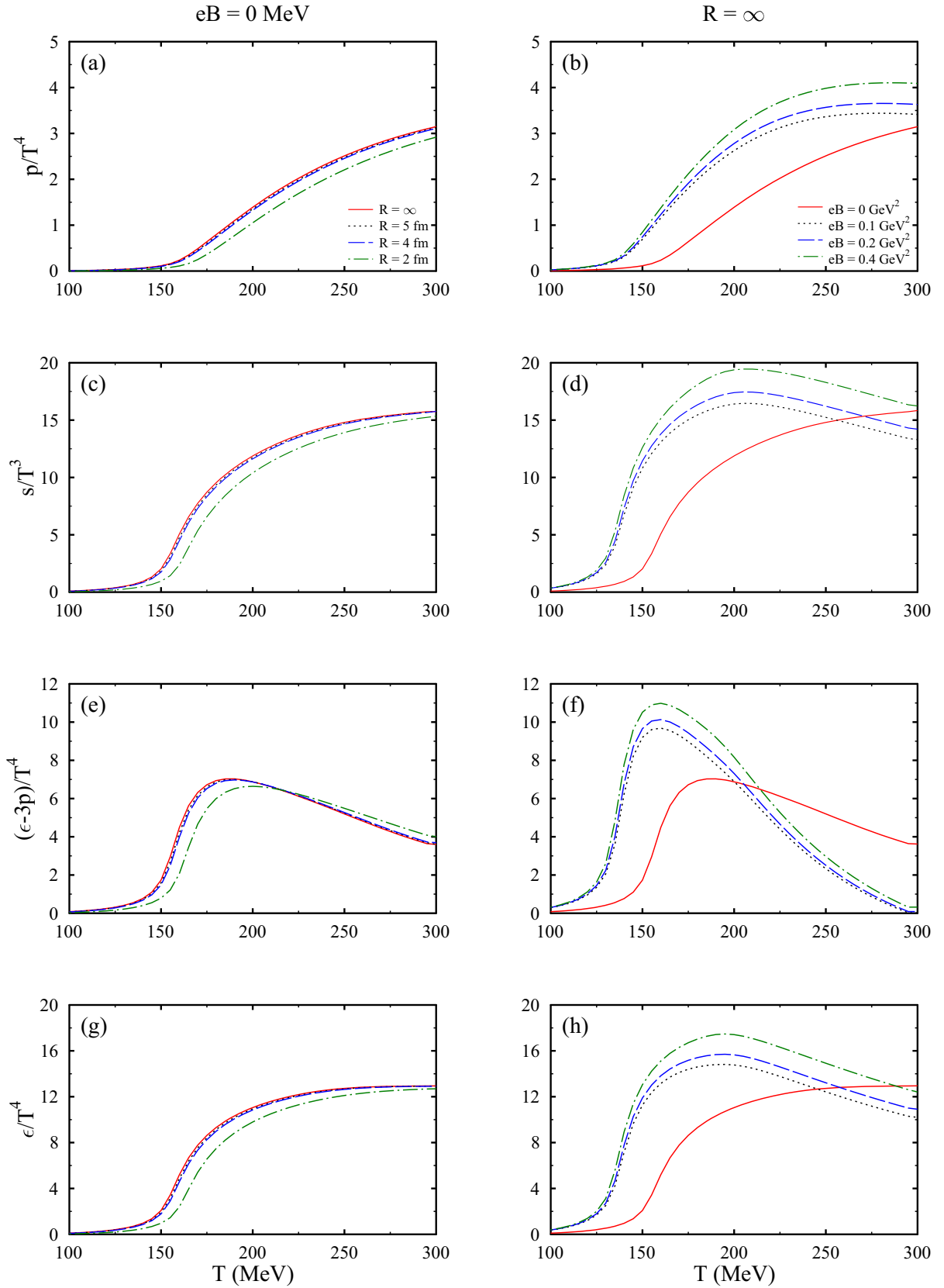


FIG. 6. The pressure density p , entropy density s , trace anomaly $(\epsilon - 3p)/T^4$, and energy density ϵ as a function of temperature for different values of length of cubic volume (R) and magnetic field (eB) at baryonic chemical potential $\mu_B = 200$ MeV, isospin chemical potential $\mu_I = 80$ MeV, and strangeness chemical potential $\mu_S = 200$ MeV.

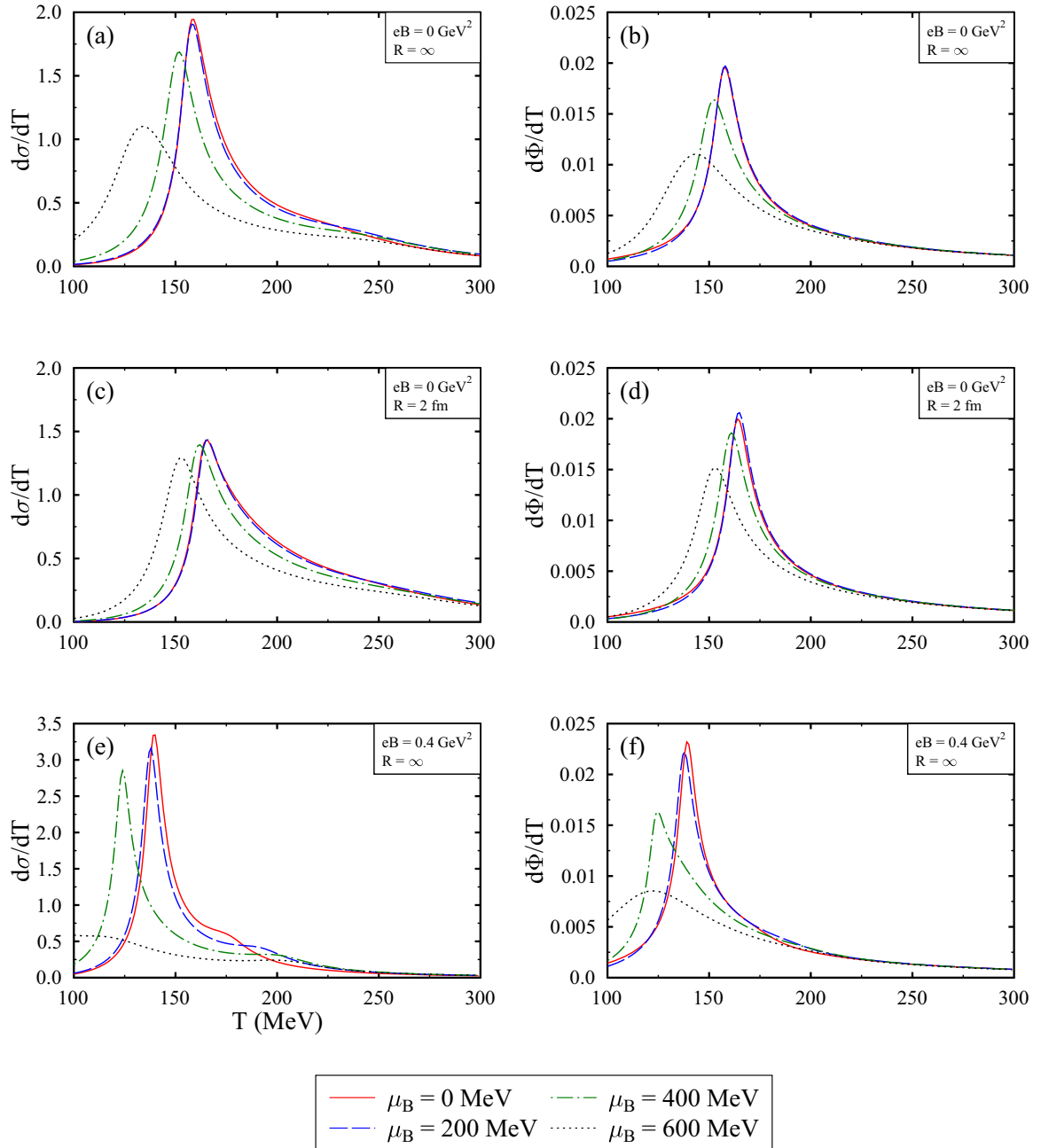


FIG. 7. The derivative of scalar field σ and Polyakov loop field, Φ shown as a function of temperature T , varying values of length of cubic volume R , and magnetic field eB . The baryonic chemical potential $\mu_B = 0, 200, 400, 600$ MeV, isospin chemical potential $\mu_I = 80$ MeV, and strangeness chemical potential $\mu_S = 200$ MeV.

chemical potential for $T > 200$ MeV. The scalar isovector field δ induces the isospin asymmetry to the medium. In the quark matter, the magnitude of δ field is derived from the difference between the scalar densities of up and down quark. Hence, in Fig. 1(e), the value of δ is almost zero for the vanishing magnetic field and baryonic chemical potential. On the other side, we see nonzero magnitude of δ field for a finite value of baryonic chemical potential and vanishing magnetic field. The asymmetry in the medium at zero magnetic field value is introduced by finite isospin chemical potential. Due to the Landau quantization in the presence of the external

magnetic field, we observe an enhancement in the magnitude of δ field for a given value of T and μ_B . Figures 1(g) and 1(h) show the variation of the dilaton field, which incorporates the property of trace anomaly in the quark mean-field model. It shows the same behavior as σ and ζ fields. It first remains constant up to a certain value of temperature and then decreases monotonically with a further temperature rise.

In Fig. 2, for the vanishing value of baryonic chemical potential, both Φ and $\bar{\Phi}$ are same for varying temperature and magnetic field values. The value of Φ and $\bar{\Phi}$ is nearly zero in the low temperature region indicating the confined state

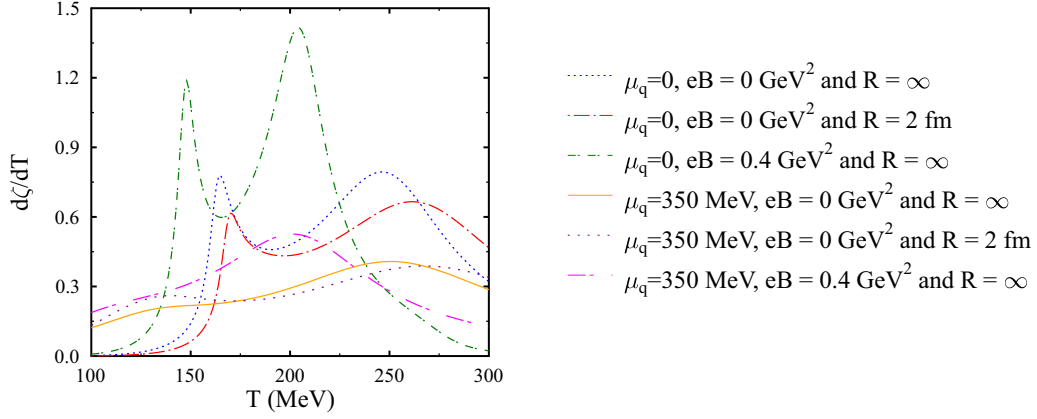


FIG. 8. The derivative of strange scalar field ζ shown as a function of temperature T for $\mu_q = 0, 350 \text{ MeV}$ at varying values of length of cubic volume R and magnetic field eB .

for a given value of μ_B . With an increase in the temperature, the value of Φ and $\bar{\Phi}$ increases due to the conversion from a confined hadronic state to a deconfined state. At nonzero magnetic field value, Polyakov loop fields show an increase for a given value of temperature and baryonic chemical potential. On further increasing the magnetic field, no significant change is observed. With the increase in the value of baryonic

chemical potential, there is a slight decrease in values of deconfinement order parameters that might indicate the decrease in deconfinement transition temperature.

Figures 3 and 4 depict the variation of $\sigma, \zeta, \delta, \chi$ fields and Polyakov loop fields Φ and $\bar{\Phi}$ as a function of temperature T , for baryonic chemical potential $\mu_B = 0$ and 200 MeV for varying system sizes. We observe that the magnitude of $\sigma,$

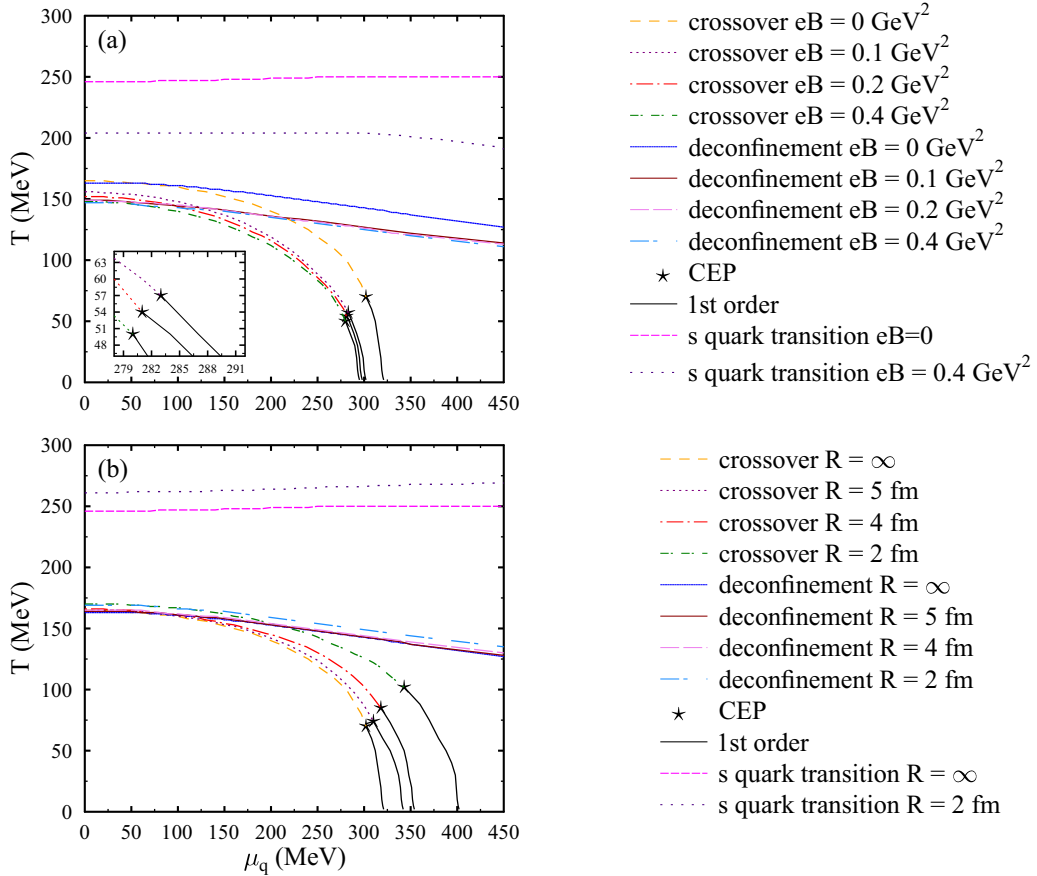


FIG. 9. In the above panel, the $T - \mu_q$ phase diagram for $eB = 0, 0.1, 0.2,$ and 0.4 GeV^2 at infinite value of length of cubic volume (R) has been plotted. In the below panel, we show the phase diagram for various cubic length $R = \infty, 5, 4,$ and 2 fm and zero value of magnetic field (eB).

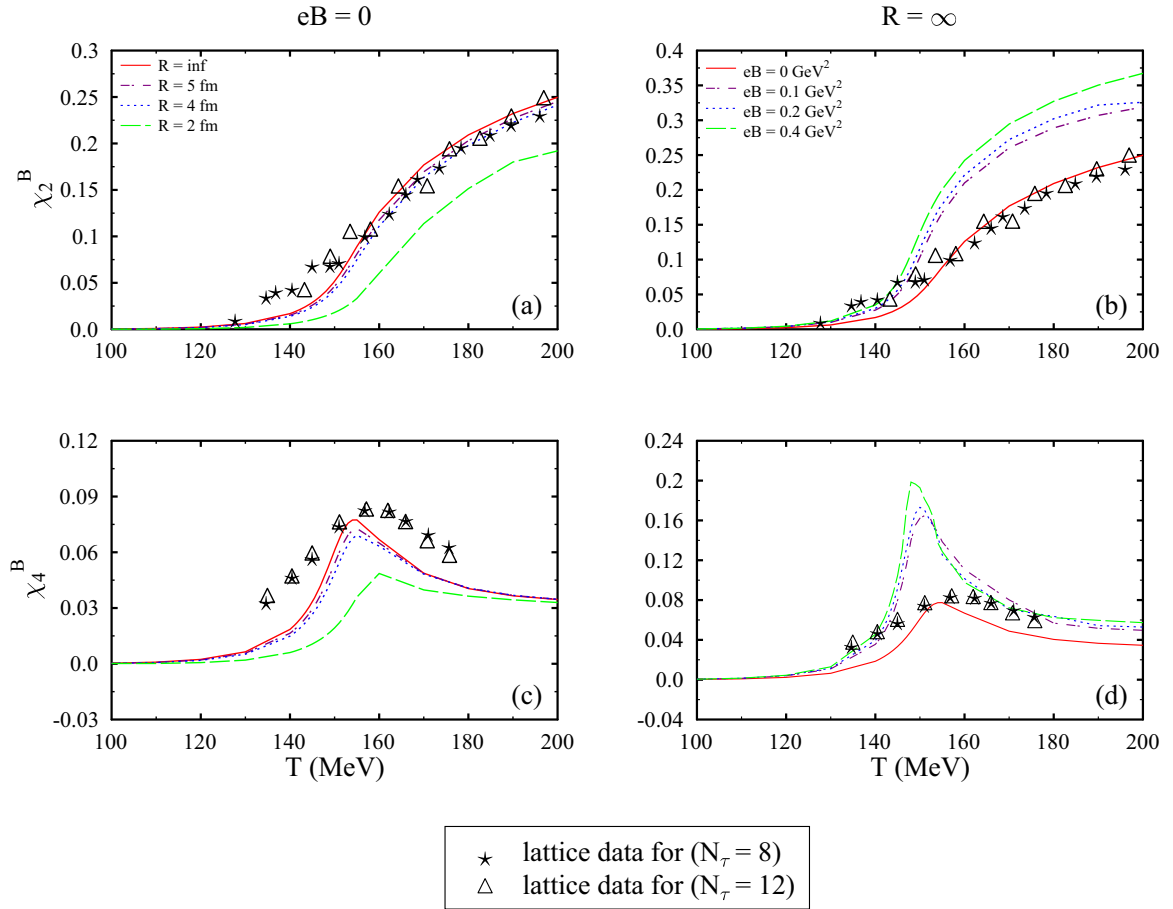


FIG. 10. The second order baryon number susceptibility (χ_2^B) and fourth order baryon number susceptibility (χ_4^B) as a function of temperature for varying value of system size (R) and magnetic field (eB). The data has been compared with lattice data.

ζ , and χ fields increases with the decrease in the system volume for a given temperature value and baryonic chemical potential. The inflection point for these fields is shifted to higher temperature value with reducing system size, which may signify the shift of pseudocritical temperature to higher values with a decrease in the system size. Similar results have been obtained for decreasing system volume by employing the PQM model in [58,59]. The perceptible volume effects are observable only for $R \leq 5$ fm [111]. There is no significant change in the δ field values for $R = 5, 4$ fm because the scalar densities of u and d quarks remain almost same for zero value of baryonic chemical potential. Although, a shift of local maxima to higher temperature value for $R = 2$ fm at finite value of isospin chemical potential is observed. The finite value of isospin potential here contributes the very low values of δ field and hence asymmetry. For finite value of μ_B , we see an increase in the value of local maxima of δ field for a fixed system size. The maximum value of δ field decreases with the decrease in the system size for both finite and zero value of μ_B while the peak shifts to a higher value of temperature.

In Fig. 4, we perceive a fall in the magnitude of deconfinement parameters with decrease in system volume, which is in contrast to that observed with the finite magnetic field.

An increase in the magnitude of Φ and $\bar{\Phi}$ is observed for increasing magnetic field. But this decrement in values of Polyakov loop conjugates for decreasing system size is more appreciable in case of $R = 2$ fm.

Figure 5 depicts the modification of quark masses in the effective mean field as a function of temperature T for different values of length of cubic volume (R) and magnetic field (eB). The effective masses of quarks are derived from the coupling of scalar fields σ , ζ and δ with the quarks. As already discussed, the magnitude of scalar fields increases due to a decrease in the system volume, hence we observe an increase in the effective mass of quarks for a given value of temperature and chemical potential. On the other hand, due to the fall in magnitude of scalar fields with the increasing magnetic field, quark masses are reduced due to inverse magnetic catalysis. This happens as a result of the suppression of quark condensates with the increasing magnetic field. Also, the sudden fall in value of masses of quarks, signifying the change in degrees of freedom, seems to happen at a higher temperature with decreasing system size, whereas the pseudocritical temperature shifts to a lower value of temperature with the rise in the magnetic field.

In Fig. 6, we have studied the variations of thermodynamic quantities, pressure density p , entropy density s , trace

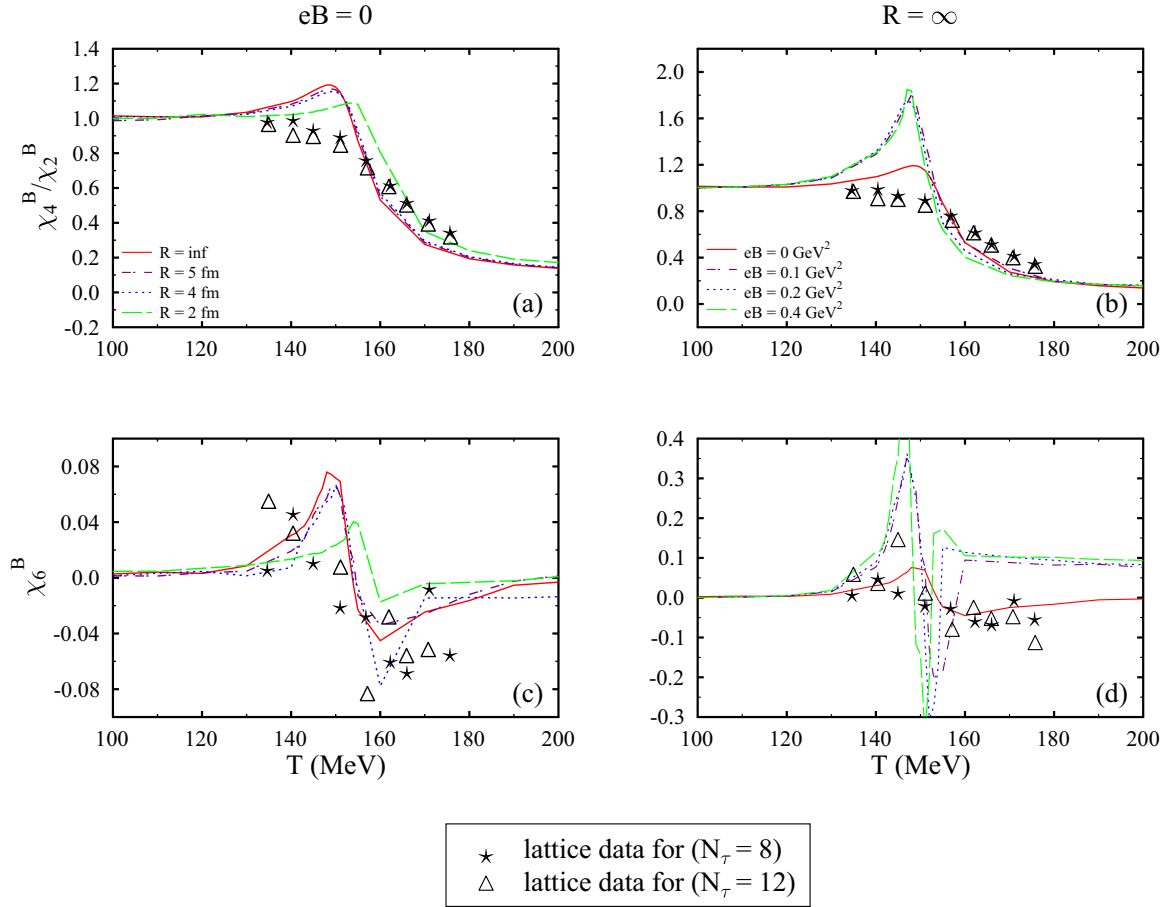


FIG. 11. The kurtosis (χ_4^B/χ_2^B) and sixth order baryon number susceptibility (χ_6^B) as a function of temperature for varying value of system size (R) and magnetic field (eB). The data have been compared with lattice data.

anomaly $(\epsilon - 3p)/T^4$, and energy density ϵ as a function of temperature for varying values of system size and magnetic field at the baryonic chemical potential μ_B fixed at 200 MeV. A sharp rise in the value of p , s , $(\epsilon - 3p)/T^4$, and ϵ is noticed in the vicinity of the transition temperature. A similar trend for thermodynamic quantities has been observed in many different studies [68,89,94]. The value of trace anomaly is quite small for low temperature values, due to the confinement of quarks. For high values of temperature, interaction strength becomes weaker and quarks are in the free state. The values increase sharply at transition temperature for all thermodynamic quantities and then advance to the ideal gas limit. The Stefan-Boltzmann (SB) limit depends on the number of flavors considered in the study [66,89]. For decrease in the system size, there is a slight fall in pressure and entropy density values. A similar impact of finite volume on thermodynamic properties of quark matter has also been reported in [97]. So we conclude that there is an enhancement in the thermodynamic quantities with the increase in magnetic field strength, while there is a reduction in values of thermodynamic properties for decreasing system volume for temperature range 100–240 MeV. There is a change in the trend for trace anomaly at higher values in case of varying system sizes. Also, the variation of entropy density, trace

anomaly and energy density with the temperature at different magnetic field values changes for $T > 240$ MeV.

In Fig. 7, we have plotted the derivative of non-strange scalar field σ and Polyakov loop variable Φ as a function of temperature for varying magnetic fields and system sizes. There are three types of phase transitions in the QCD phase diagram, first is the chiral symmetry restoration of u and d quarks, second chiral symmetry restoration of s quarks, and the third is deconfinement transition. The value of critical temperatures for these three phase transition may be referred as T_c^q , T_c^s , and T_c^d , respectively. If the number of peaks is one in temperature derivative of order parameters, then the critical temperature is obtained by the location of the peak. At zero value of the magnetic field and infinite system size, the value of $T_c^q \approx 160$ MeV and $T_c^d \approx 158$ MeV for vanishing values of baryonic chemical potential. When we further increase the baryonic chemical potential, the chiral transition temperature shifts to a lower temperature value. In all the cases, significant change in critical temperature value is observed for $\mu_B > 200$ MeV. For finite value of system size and zero magnetic field, we see a shift of peak to higher value of temperature for a given value of baryonic chemical potential. On the contrary, relocation of peak to lower temperature value is seen for finite value of magnetic field. A similar trend of chiral transition

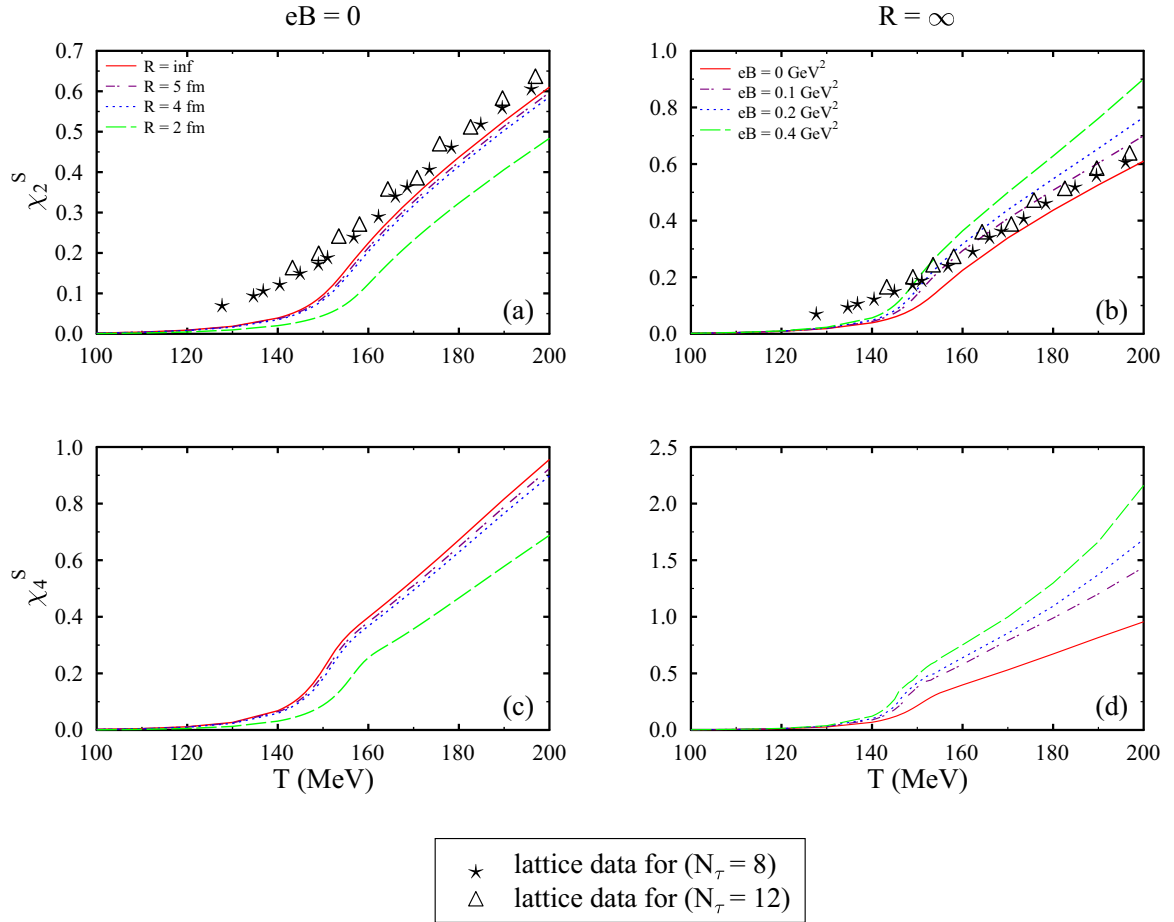


FIG. 12. The second order strangeness number susceptibility (χ_2^s) and fourth order strangeness number susceptibility (χ_4^s) as a function of temperature for varying value of system size (R) and magnetic field (eB). The data have been compared with lattice data.

temperature and deconfinement transition temperature is perceived in all scenarios of magnetic field and system volume.

In Fig. 8, we have plotted the derivative of strange scalar field ζ for different system sizes and magnetic field values. For the derivative of strange fields ζ , two peaks are observed at zero value of quark chemical potential. The first peak coincides with the value of T_c^q of light quarks whereas the second peak corresponds to the chiral phase transition for s quark. When there are two peaks in temperature derivative of condensate, for the chiral phase transition, the critical temperature can be obtained by the peak temperature analogous to $\sigma(T)/\sigma(T=0) < 1/2$, while for deconfinement phase transition, it can be obtained by using the relation $\Phi(T)/\Phi(T \rightarrow \infty) > 1/2$ [100]. At higher values of quark chemical potential, the first peak vanishes as in case of $\mu_q = 350$ MeV.

In Fig. 9, we have plotted the QCD phase diagram at finite values of magnetic field and varying system sizes. The three types of phase transitions, i.e., the phase transition for light u and d quarks, the phase transition of s quarks and deconfinement phase transition corresponding to Polyakov fields are shown in this figure. For light quarks, at zero value of magnetic field and infinite system size [Fig. 9(a)], $(T_{CP}, \mu_{q(CP)}) = (70, 302)$ MeV. For infinite system size and $eB = 0.1 \text{ GeV}^2$, the value of $T_{CP} = 57$ MeV and $\mu_{q(CP)} =$

283 MeV. The critical point $(T_{CP}, \mu_{q(CP)}) = (54, 281)$ MeV for $eB = 0.2 \text{ GeV}^2$ and $(T_{CP}, \mu_{q(CP)}) = (50, 280)$ MeV for $eB = 0.4 \text{ GeV}^2$ for infinite system volume. The critical-point values for varying magnetic field strength are listed in Table III. Hence we can conclude that critical point shifts to lower value of temperature and quark chemical potential due to increasing magnetic field. By Fig. 9(b), it is clear that with decrease in value of length of cubic volume, the critical-point moves towards higher value of temperature and quark chemical potential. For magnetic field, $eB = 0$ and $R = 5 \text{ fm}$, the value of $T_{CP} = 74$ MeV and $\mu_{q(CP)} = 310$ MeV. The critical point $(T_{CP}, \mu_{q(CP)}) = (85, 318)$ MeV for $R = 4 \text{ fm}$ and $(T_{CP}, \mu_{q(CP)}) = (102, 343)$ MeV for $R = 2 \text{ fm}$ at zero

TABLE III. The value of critical-temperature and quark chemical potential for finite values of magnetic field.

eB (GeV^2)	T_{CP} (MeV)	$\mu_{q(CP)}$ (MeV)
0	70	302
0.1	57	283
0.2	54	281
0.4	50	280

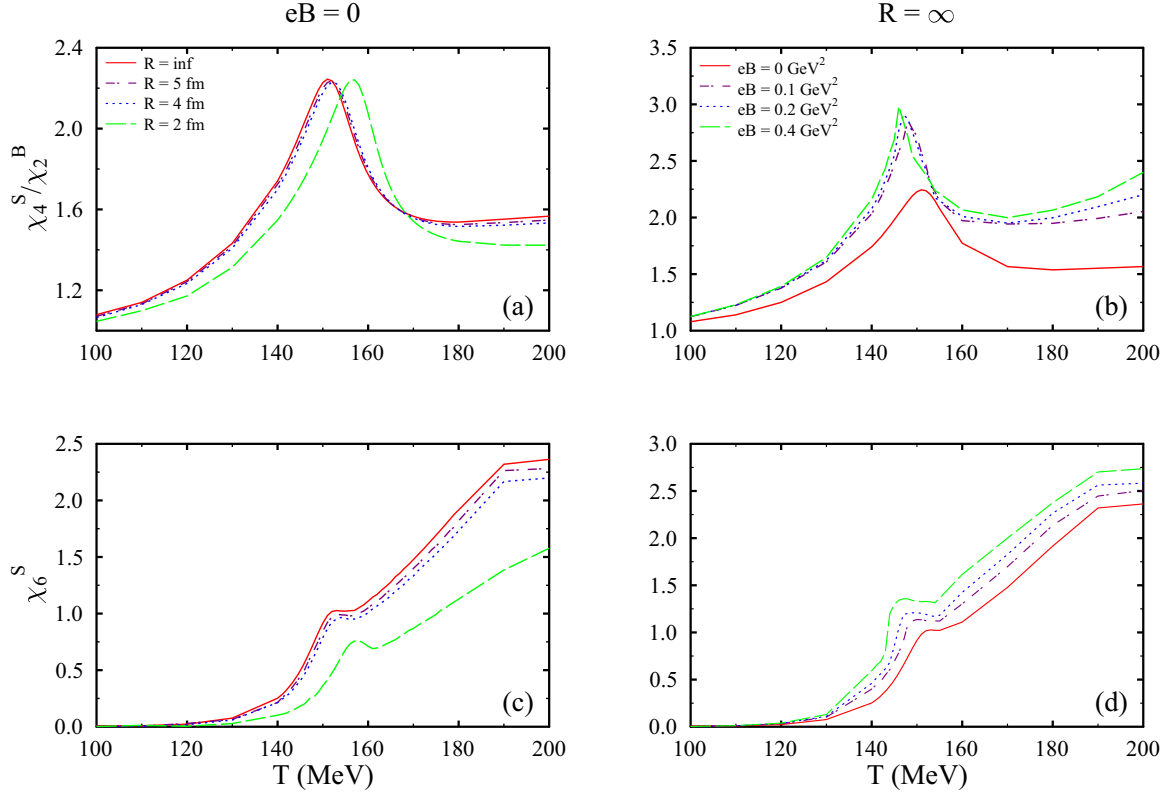


FIG. 13. The kurtosis (χ_4^S/χ_2^S) and sixth order strangeness number susceptibility (χ_6^S) as a function of temperature for varying value of system size (R) and magnetic field (eB).

value of the magnetic field. The critical-point values for different system sizes are listed in Table IV. This behavior of critical point is analogous to the one discussed in [58,59] for PLSM. The deconfinement phase boundary is shifted to higher temperature values with decreasing system size and lower temperature value with increasing magnetic field strength. The chiral phase transition for s quark and deconfinement transition is always a crossover in the QCD phase diagram [112]. On the other hand, for light quarks, the phase transition is a crossover till the critical-point and changes to first-order phase transition at higher values of quark chemical potential. The chiral phase boundary for s quark follows the same trend as deconfinement phase transition in case of varying system size and magnetic field. The phase boundary is thus modified due to finite volume and finite magnetic field. It is to be noted that the value of isospin and strangeness chemical potential is considered to be zero while plotting the phase diagram. In earlier studies of the PCQMF model, the

TABLE IV. The value of critical-temperature and quark chemical potential for finite values of system size.

R (fm)	T_{CP} (MeV)	$\mu_{q(CP)}$ (MeV)
∞	70	302
5	74	310
4	85	318
2	102	343

phase boundary was concluded to shift towards low values of temperature and higher values of quark chemical potential for increasing vector interaction, whereas a relocation of critical point to lower temperature and quark chemical potential values have been reported for increasing isospin chemical potential [68].

B. Susceptibilities of conserved charges

In this section, we will discuss the susceptibilities of baryon number, strangeness number, and charge number for varying values of magnetic field and finite system size. These susceptibilities have been calculated by expanding Taylor's series around $\mu_B = \mu_S = \mu_Q = 0$. Susceptibilities of conserved charges carry information about the QCD critical point and hence are important to study in the QCD phase diagram. It is due to the fact that above mentioned charges are conserved during the evolution of matter produced in heavy ion collisions and hence their fluctuations can be extracted by event-by-event analysis of the experiments [41,113]. In Fig. 10, we have plotted the variation of the second- and fourth-order baryon number susceptibility (χ_2^B and χ_4^B) as a function of temperature for different values of system size (R) and magnetic field (eB). Susceptibilities have been calculated by using the Taylor series expansion discussed earlier in Sec. II B at vanishing chemical potential. The results obtained in the current study have been compared with lattice data for zero value of the magnetic field and infinite system size [114,115]. In the left panel, we can clearly see that value of χ_2^B

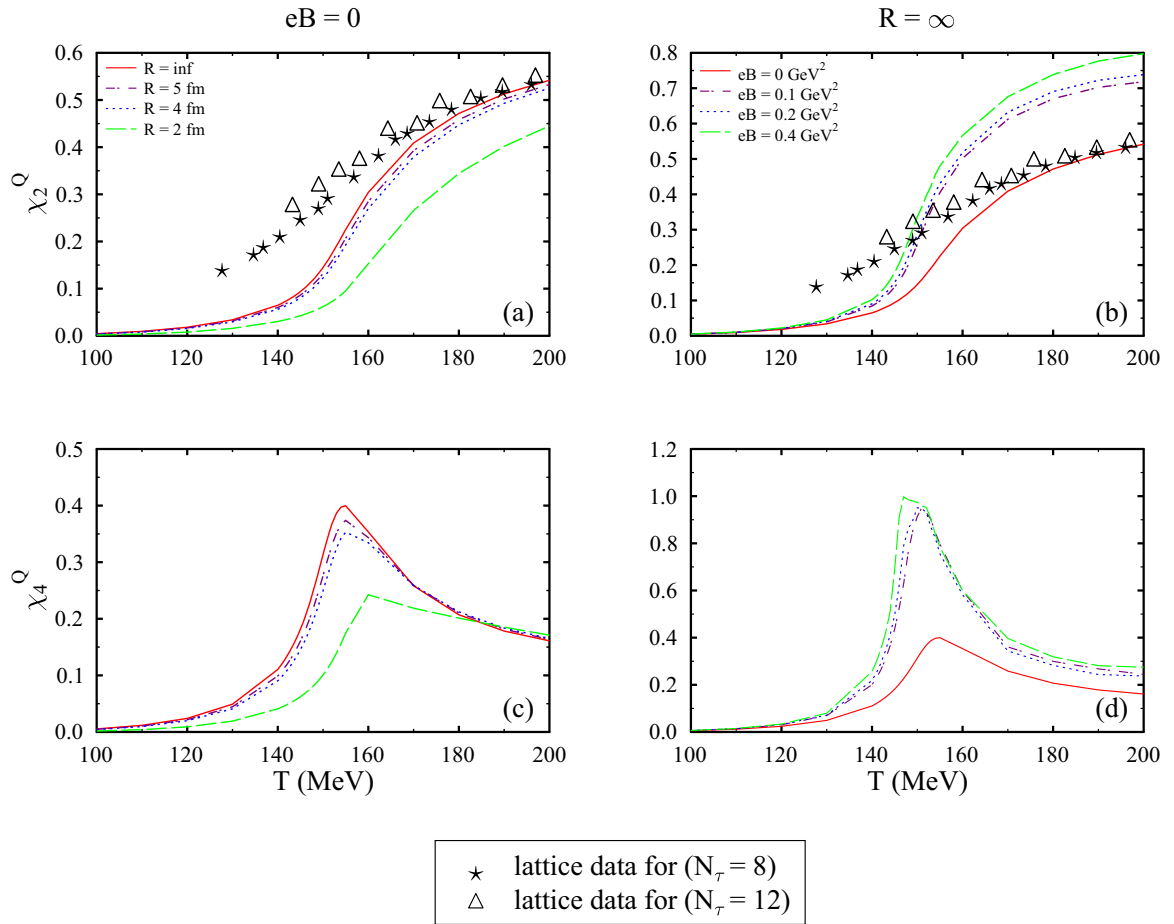


FIG. 14. The second order charge number susceptibility (χ_2^Q) and fourth order charge number susceptibility (χ_4^Q) as a function of temperature for varying values of system size (R) and magnetic field (eB). The data have been compared with lattice data.

and χ_4^B decreases with the decrease in the system volume. As a function of T , a sudden increase in the value of susceptibilities is observed near the transition regime. This enhancement of susceptibilities may be an important signature of QCD critical point. This decrease in susceptibility of conserved charge due to decreasing system volume has also been observed in the PQM model [58]. On the other hand, there is an increase in the value of susceptibilities with increase in value of magnetic field. This is attributed to the “inverse magnetic catalysis”, which have been discussed earlier. The susceptibilities of conserved charges in external magnetic field have been studied in [39]. We observe that the thermodynamic quantities studied in the previous section show a rise with increment in external magnetic field but decreases with decreasing system size for $T < 220$ MeV. When the transition becomes an exact second order, the fluctuations of conserved charges must be divergent in nature [39].

In Fig. 11, we have plotted the kurtosis (χ_4^B/χ_2^B) and sixth order susceptibility (χ_6^B) of baryon number. Kurtosis is considered as crucial observable in order to investigate the location of CEP owing to its sensitivity for both chiral and deconfinement transitions [116,117]. In low temperature range, (χ_4^B/χ_2^B) is approximately one which represents the confined state of quarks whereas its value drops to ≈ 0.1 at high temperatures due to the change in degrees of freedom

of quarks. It is not possible to determine skewness by using Taylor series expansion for zero value of baryonic chemical potential [109]. This is due to the disintegration of odd terms in Taylor series expansion as a result of charge-parity symmetry. The (χ_4^B/χ_2^B) and (χ_6^B) show a similar trend for finite values of magnetic field and volume. There is also a shift in the peak of kurtosis towards higher temperature as system size decreases which confirms the relocation of transition temperature towards higher values. On the other hand, we have opposite shift towards low temperatures with increasing magnetic field values.

Figures 12 and 13 display the variation of susceptibilities of strangeness number as a function of temperature. In the confined state with hadrons as degrees of freedom, mainly kaons contribute to the strangeness of system. This happens because of the suppressed production of heavy strange mesons in this phase [118]. But in the deconfined phase, strangeness is contributed by low mass hadrons. This results in the maximization of fluctuations of strangeness number and hence plays a vital role in investigating deconfinement transition [66]. The trend of χ_2^S is similar to that of χ_2^B , it increases monotonically with increase in temperature. It has been observed in PNJL model that impact of varying magnetic field is more pronounced in case of s quarks, especially for low order fluctuations [39]. A peaked structure is observed in the

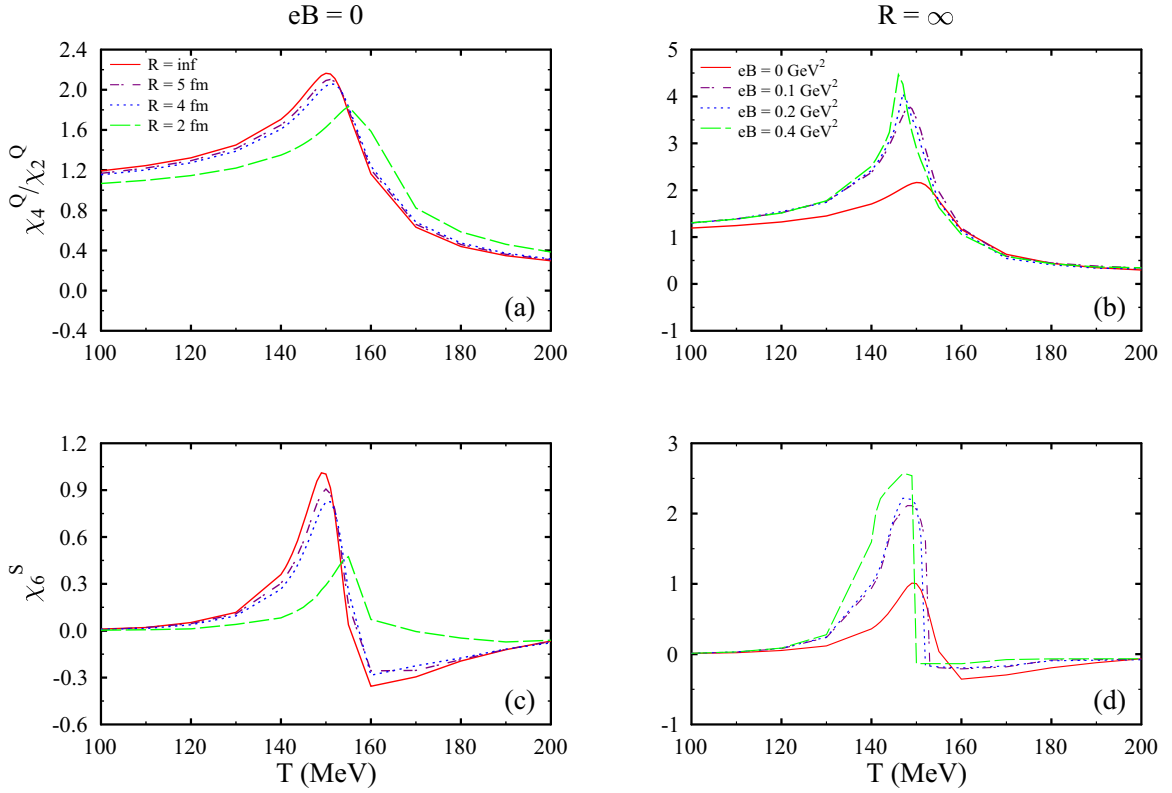


FIG. 15. The kurtosis (χ_4^Q/χ_2^Q) and sixth order charge number susceptibility (χ_6^Q) as a function of temperature for varying value of system size (R) and magnetic field (eB).

kurtosis of strangeness number in the transition regime. We observe a sharp rise in the second, fourth and sixth order strangeness number susceptibilities in temperature range of 140–160 MeV, signaling the change of phase from confined hadronic to deconfined QGP phase. In Figs. 14 and 15 we have shown charge number fluctuations as a temperature function. The second order susceptibilities of all conserved charges follow the similar smooth trend with increasing values of temperature. There is a considerable rise in value of susceptibility value near the phase transition region with increasing magnetic field whereas the magnitude decreases with decreasing system size. Also there is a shift towards lower temperature for different magnetic field values but an opposite dislocation to higher temperature is observed by reducing system volume. The effect of external magnetic field on the fluctuations of conserved charges have been shown to enhance the magnitude of susceptibilities in the transition regime in the PNJL model [39]. All the above results are in fair agreement with the lattice QCD simulations for χ_2^Q at high temperature.

IV. SUMMARY

We have analyzed the impact of finite volume and external magnetic field on the thermodynamic properties using Polyakov loop extended chiral SU(3) quark mean field model in the asymmetric quark matter. The impact of external magnetic field and finite system size on the phase diagram of QCD have been investigated by inspecting the variation of scalar and vector fields along with Polyakov loop variables at different values of temperature and chemical potential.

Various thermodynamic properties like pressure density, energy density, entropy density, trace anomaly property and quark masses have been studied for varying system size and magnetic field. We have observed an increase in magnitude of thermodynamic quantities studied in the current work with the increasing magnetic field in temperature range 125–250 MeV whereas there is a fall in the magnitude with decreasing system size. Phase boundary is found to shift towards lower values of temperature and quark chemical potential with increasing magnetic field and higher value of temperature and quark chemical potential for decreasing system volume. The fluctuations of conserved charges, baryon number, strangeness number, and charge number have been calculated for various values of magnetic field and length of cubic volume. Susceptibilities of conserved charges are found to be enhanced in the regime of critical-point. The peaked structure of quartic susceptibilities becomes more and more pronounced with the rise in magnetic field strength. These fluctuations can be deduced from event-by-event inspection of the experimental data and hence play a significant role in the determination of CEP. The results obtained have been compared with the lattice QCD simulations data for zero value of magnetic field and infinite system size. In future work, we will calculate the fluctuations of conserved charges for varying values of magnetic field and system volume for non-zero value of chemical potential. The functional renormalization approach can be employed to study thermodynamic variables of quark matter beyond mean field [119]. The work will be extended in the future to study the higher order cumulants using automatic differentiation [120].

ACKNOWLEDGMENTS

The authors sincerely acknowledge the support towards this work from the Ministry of Science and Human Resources (MHRD), Government of India via Institute

fellowship under the National Institute of Technology Jalandhar. A.K. sincerely acknowledges the DST-SERB, Government of India for funding of research Project No. CRG/2019/000096.

- [1] W. Busza, K. Rajagopal, and W. Van Der Schee, *Annu. Rev. Nucl. Part. Sci.* **68**, 339 (2018).
- [2] A. Ohnishi, *Prog. Theor. Phys. Suppl.* **193**, 1 (2012).
- [3] A. Pandav, D. Mallick, and B. Mohanty, *Prog. Part. Nucl. Phys.* **125**, 103960 (2022).
- [4] L. Kumar *et al.* (STAR Collaboration), *Nucl. Phys. A* **904–905**, 256c (2013).
- [5] G. Odyniec, *J. Phys. G: Nucl. Part. Phys.* **37**, 094028 (2010).
- [6] O. Brüning, H. Burkhardt, and S. Myers, *Prog. Part. Nucl. Phys.* **67**, 705 (2012).
- [7] A. Sissakian, A. Sorin *et al.* (NICA Collaboration), *J. Phys. G: Nucl. Part. Phys.* **36**, 064069 (2009).
- [8] M. Durante, P. Indelicato, B. Jonson, V. Koch, K. Langanke, U.-G. Meißner, E. Nappi, T. Nilsson, T. Stöhlker, E. Widmann *et al.*, *Phys. Scr.* **94**, 033001 (2019).
- [9] M. Stephanov, [arXiv:hep-lat/0701002](https://arxiv.org/abs/hep-lat/0701002).
- [10] C. DeTar and U. Heller, *Eur. Phys. J. A* **41**, 405 (2009).
- [11] R. Gupta, *AIP Conference Proceedings CONF-981188* (American Institute of Physics, New York, 1999), Vol. 490, pp. 3–9.
- [12] Y. Aoki, G. Endrődi, Z. Fodor, S. D. Katz, and K. K. Szabó, *Nature* **443**, 675 (2006).
- [13] J. N. Guenther, *Eur. Phys. J. A* **57**, 136 (2021).
- [14] V. Goy, V. Bornyakov, D. Boyda, A. Molochkov, A. Nakamura, A. Nikolaev, and V. Zakharov, *Prog. Theor. Exp. Phys.* **2017**, 031D01 (2017).
- [15] S. Muroya, A. Nakamura, C. Nonaka, and T. Takaishi, *Prog. Theor. Phys.* **110**, 615 (2003).
- [16] J. Danzer, C. Gattlinger, L. Liptak, and M. Marinkovic, *Phys. Lett. B* **682**, 240 (2009).
- [17] Z. Fodor and S. D. Katz, *Phys. Lett. B* **534**, 87 (2002).
- [18] S. Ejiri, *Phys. Rev. D* **78**, 074507 (2008).
- [19] Y. Hatta and T. Ikeda, *Phys. Rev. D* **67**, 014028 (2003).
- [20] Z. Fodor and S. D. Katz, *J. High Energy Phys.* **04** (2004) 050.
- [21] M. Stephanov, *Prog. Theor. Phys. Suppl.* **153**, 139 (2004).
- [22] R. A. Lacey, *Phys. Rev. Lett.* **114**, 142301 (2015).
- [23] D. Tlusty, [arXiv:1810.04767](https://arxiv.org/abs/1810.04767).
- [24] M. Stephanov, *Journal of Physics: Conference Series* (IOP Publishing, Bristol, 2005), Vol. 27.
- [25] P. Garg, D. Mishra, P. Netrakanti, B. Mohanty, A. Mohanty, B. Singh, and N. Xu, *Phys. Lett. B* **726**, 691 (2013).
- [26] P. Maris and C. D. Roberts, *Int. J. Mod. Phys. E* **12**, 297 (2003).
- [27] P. Papazoglou, S. Schramm, J. Schaffner-Bielich, H. Stocker, and W. Greiner, *Phys. Rev. C* **57**, 2576 (1998).
- [28] R. D. Bowler and M. Birse, *Nucl. Phys. A* **582**, 655 (1995).
- [29] B.-J. Schaefer, J. M. Pawłowski, and J. Wambach, *Phys. Rev. D* **76**, 074023 (2007).
- [30] K. Kashiwa, H. Kouno, M. Matsuzaki, and M. Yahiro, *Phys. Lett. B* **662**, 26 (2008).
- [31] N. Dupuis, L. Canet, A. Eichhorn, W. Metzner, J. M. Pawłowski, M. Tissier, and N. Wschebor, *Phys. Rep.* **910**, 1 (2021).
- [32] E. Harrison, *Phys. Rev. Lett.* **30**, 188 (1973).
- [33] K. Enqvist and P. Olesen, *Phys. Lett. B* **319**, 178 (1993).
- [34] G. Inghirami, M. Mace, Y. Hirono, L. Del Zanna, D. E. Kharzeev, and M. Bleicher, *Eur. Phys. J. C* **80**, 293 (2020).
- [35] D. E. Kharzeev, L. D. McLerran, and H. J. Warringa, *Nucl. Phys. A* **803**, 227 (2008).
- [36] W.-T. Deng and X.-G. Huang, *Phys. Rev. C* **85**, 044907 (2012).
- [37] T. Vachaspati, *Phys. Lett. B* **265**, 258 (1991).
- [38] C. Y. Vallgren, G. Arduini, J. Bauche, S. Calatroni, P. Chiggiato, K. Cornelis, P. C. Pinto, B. Henrist, E. Métral, H. Neupert *et al.*, *Phys. Rev. ST Accel. Beams* **14**, 071001 (2011).
- [39] W.-j. Fu, *Phys. Rev. D* **88**, 014009 (2013).
- [40] V. Skokov, A. Y. Illarionov, and V. Toneev, *Int. J. Mod. Phys. A* **24**, 5925 (2009).
- [41] B. Abelev, M. Aggarwal, Z. Ahammed, A. Alakhverdyants, B. Anderson, D. Arkhipkin, G. Averichev, J. Balewski, O. Barannikova, L. Barnby *et al.*, *Phys. Rev. Lett.* **103**, 251601 (2009).
- [42] K. Fukushima, M. Ruggieri, and R. Gatto, *Phys. Rev. D* **81**, 114031 (2010).
- [43] G. S. Bali, F. Bruckmann, G. Endrődi, Z. Fodor, S. Katz, and A. Schäfer, *Phys. Rev. D* **86**, 071502(R) (2012).
- [44] F. Bruckmann, G. Endrődi, and T. G. Kovacs, *J. High Energy Phys.* **04** (2013) 112.
- [45] I. Shushpanov and A. V. Smilga, *Phys. Lett. B* **402**, 351 (1997).
- [46] K. Klimenko, *Z. Phys. C* **54**, 323 (1992).
- [47] I. A. Shovkovy, *Strongly Interacting Matter in Magnetic Fields* (Springer, Berlin, 2013), pp. 13–49.
- [48] G. Bali, F. Bruckmann, M. Constantinou, M. Costa, G. Endrődi, Z. Fodor, S. D. Katz, S. Krieg, H. Panagopoulos, A. Schafer *et al.*, *PoS Proc. Sci.* **171**, 0197 (2013).
- [49] S. P. Klevansky and R. H. Lemmer, *Phys. Rev. D* **39**, 3478 (1989).
- [50] G. Endrődi, *J. High Energy Phys.* **04** (2013) 130.
- [51] G. Bali, F. Bruckmann, G. Endrődi, Z. Fodor, S. Katz, S. Krieg, A. Schäfer, and K. Szabo, *J. High Energy Phys.* **02** (2012) 044.
- [52] E. S. Fraga, L. F. Palhares, and P. Sorensen, *Phys. Rev. C* **84**, 011903(R) (2011).
- [53] A. Bzdak, S. Esumi, V. Koch, J. Liao, M. Stephanov, and N. Xu, *Phys. Rep.* **853**, 1 (2020).
- [54] X. Luo and N. Xu, *Nucl. Sci. Tech.* **28**, 112 (2017).
- [55] A. Bhattacharyya, S. K. Ghosh, R. Ray, K. Saha, and S. Upadhaya, *Europhys. Lett.* **116**, 52001 (2016).
- [56] M. E. Fisher and M. N. Barber, *Phys. Rev. Lett.* **28**, 1516 (1972).
- [57] E. Brézin and J. Zinn-Justin, *Nucl. Phys. B* **257**, 867 (1985).
- [58] N. Magdy, *Universe* **5**, 94 (2019).
- [59] N. Magdy, M. Csanád, and R. A. Lacey, *J. Phys. G: Nucl. Part. Phys.* **44**, 025101 (2017).
- [60] N. B. Mata Carrizal, E. Valbuena Ordóñez, A. J. Garza Aguirre, F. J. Betancourt Sotomayor, and J. R. Morones Ibarra, *Universe* **8**, 264 (2022).

- [61] A. G. Grunfeld and G. Lugones, *Eur. Phys. J. C* **78**, 640 (2018).
- [62] O. Kiriya, *Phys. Rev. D* **72**, 054009 (2005).
- [63] Y.-P. Zhao, R.-R. Zhang, H. Zhang, and H.-S. Zong, *Chin. Phys. C* **43**, 063101 (2019).
- [64] Y.-P. Zhao, P.-L. Yin, Z.-H. Yu, and H.-S. Zong, *Nucl. Phys. B* **952**, 114919 (2020).
- [65] G. Lugones and A. G. Grunfeld, *Phys. Rev. C* **99**, 035804 (2019).
- [66] S. Borsanyi, Z. Fodor, S. D. Katz, S. Krieg, C. Ratti, and K. Szabo, *J. High Energy Phys.* **08** (2012) 053.
- [67] J. Adam, Technical Report, Brookhaven National Laboratory (BNL), Upton, NY (2020).
- [68] N. Chahal, S. Dutt, and A. Kumar, *Chin. Phys. C* **46**, 063104 (2022).
- [69] S. Chatterjee and K. A. Mohan, *Phys. Rev. D* **86**, 114021 (2012).
- [70] W. Fan, X. Luo, and H. Zong, *Chin. Phys. C* **43**, 033103 (2019).
- [71] M. Asakawa and M. Kitazawa, *Prog. Part. Nucl. Phys.* **90**, 299 (2016).
- [72] B. A. Berg and H. Wu, *Phys. Rev. D* **88**, 074507 (2013).
- [73] M. Cristoforetti, T. Hell, B. Klein, and W. Weise, *Phys. Rev. D* **81**, 114017 (2010).
- [74] H.-T. Ding, S.-T. Li, Q. Shi, and X.-D. Wang, *Eur. Phys. J. A* **57**, 202 (2021).
- [75] P. Wang, V. E. Lyubovitskij, T. Gutsche, and A. Faessler, *Phys. Rev. C* **67**, 015210 (2003).
- [76] R. Poberezhnyuk, V. Vovchenko, D. Anchishkin, and M. Gorenstein, *Int. J. Mod. Phys. E* **26**, 1750061 (2017).
- [77] P. Wang, H. Guo, Z. Zhang, Y. Yu, R. Su, and H. Song, *Nucl. Phys. A* **705**, 455 (2002).
- [78] P. Wang, D. Leinweber, A. Thomas, and A. Williams, *Nucl. Phys. A* **744**, 273 (2004).
- [79] P. Wang, Z. Zhang, Y. Yu, R. Su, and Q. Song, *Nucl. Phys. A* **688**, 791 (2001).
- [80] K. Fukushima and V. Skokov, *Prog. Part. Nucl. Phys.* **96**, 154 (2017).
- [81] H. Hansen, R. Stiele, and P. Costa, *Phys. Rev. D* **101**, 094001 (2020).
- [82] C. Ratti, M. A. Thaler, and W. Weise, *Phys. Rev. D* **73**, 014019 (2006).
- [83] T. K. Herbst, J. M. Pawłowski, and B.-J. Schaefer, *Phys. Lett. B* **696**, 58 (2011).
- [84] W.-j. Fu, X. Luo, J. M. Pawłowski, F. Rennecke, R. Wen, and S. Yin, *Phys. Rev. D* **104**, 094047 (2021).
- [85] M. Bando, T. Kugo, and K. Yamawaki, *Phys. Rep.* **164**, 217 (1988).
- [86] S. Weinberg, *Phys. Rev.* **166**, 1568 (1968).
- [87] D. Kharzeev, E. Levin, and K. Tuchin, *J. High Energy Phys.* **06** (2009) 055.
- [88] A. Beekman, L. Rademaker, and J. van Wezel, *SciPost Physics Lecture Notes* **11** (2019).
- [89] M. Kumari and A. Kumar, *Eur. Phys. J. Plus* **136**, 19 (2021).
- [90] P. Papazoglou, D. Zschesche, S. Schramm, J. Schaffner-Bielich, H. Stöcker, and W. Greiner, *Phys. Rev. C* **59**, 411 (1999).
- [91] B.-J. Schaefer, M. Wagner, and J. Wambach, *Phys. Rev. D* **81**, 074013 (2010).
- [92] S. Rossner, C. Ratti, and W. Weise, *Phys. Rev. D* **75**, 034007 (2007).
- [93] M. Fukugita, M. Okawa, and A. Ukawa, *Nucl. Phys. B* **337**, 181 (1990).
- [94] A. N. Tawfik and N. Magdy, *Phys. Rev. C* **90**, 015204 (2014).
- [95] M. Ferreira, P. Costa, O. Lourenço, T. Frederico, and C. Providência, *Phys. Rev. D* **89**, 116011 (2014).
- [96] A. N. Tawfik, A. M. Diab, and M. Hussein, *J. Exp. Theor. Phys.* **126**, 620 (2018).
- [97] A. Bhattacharyya, P. Deb, S. K. Ghosh, R. Ray, and S. Sur, *Phys. Rev. D* **87**, 054009 (2013).
- [98] A. Bhattacharyya, R. Ray, S. Samanta, and S. Sur, *Phys. Rev. C* **91**, 041901(R) (2015).
- [99] V. Skokov, B. Friman, E. Nakano, K. Redlich, and B.-J. Schaefer, *Phys. Rev. D* **82**, 034029 (2010).
- [100] H. Mao, J. Jin, and M. Huang, *J. Phys. G: Nucl. Part. Phys.* **37**, 035001 (2010).
- [101] S. Chatterjee and K. A. Mohan, *Phys. Rev. D* **85**, 074018 (2012).
- [102] U. S. Gupta and V. K. Tiwari, *Phys. Rev. D* **85**, 014010 (2012).
- [103] W. Ping, Z. Zong-Ye, and Y. You-Wen, *Commun. Theor. Phys.* **36**, 71 (2001).
- [104] G.-y. Shao, Z.-d. Tang, X.-y. Gao, and W.-b. He, *Eur. Phys. J. C* **78**, 138 (2018).
- [105] M. Cheng, P. Hegde, C. Jung, F. Karsch, O. Kaczmarek, E. Laermann, R. Mawhinney, C. Miao, P. Petreczky, C. Schmidt *et al.*, *Phys. Rev. D* **79**, 074505 (2009).
- [106] V. Skokov, B. Friman, F. Karsch, and K. Redlich, *J. Phys. G: Nucl. Part. Phys.* **38**, 124102 (2011).
- [107] P. Isserstedt, M. Buballa, C. S. Fischer, and P. J. Gunkel, *Journal of Physics: Conference Series* (IOP Publishing, Bristol, 2020), Vol. 1667, p. 012015.
- [108] X.-Y. Xin, S.-X. Qin, and Y.-X. Liu, *Phys. Rev. D* **90**, 076006 (2014).
- [109] S. K. Ghosh, T. K. Mukherjee, M. G. Mustafa, and R. Ray, *Phys. Rev. D* **73**, 114007 (2006).
- [110] C. Schmidt, *Prog. Theor. Phys. Suppl.* **186**, 563 (2010).
- [111] J. Bernhardt, C. S. Fischer, P. Isserstedt, and B.-J. Schaefer, *Phys. Rev. D* **104**, 074035 (2021).
- [112] P. Costa and R. Pereira, *Symmetry* **11**, 507 (2019).
- [113] R. C. Hwa and X.-N. Wang, *Quark Gluon Plasma 3* (World Scientific, 2004).
- [114] A. Bazavov, T. Bhattacharya, M. Cheng, C. DeTar, H.-T. Ding, S. Gottlieb, R. Gupta, P. Hegde, U. M. Heller, F. Karsch *et al.* (HotQCD Collaboration), *Phys. Rev. D* **85**, 054503 (2012).
- [115] A. Bazavov, D. Bollweg, H.-T. Ding, P. Enns, J. Goswami, P. Hegde, O. Kaczmarek, F. Karsch, R. Larsen, S. Mukherjee *et al.*, *Phys. Rev. D* **101**, 074502 (2020).
- [116] S. Ejiri, F. Karsch, and K. Redlich, *Phys. Lett. B* **633**, 275 (2006).
- [117] B. Stokić, B. Friman, and K. Redlich, *Phys. Lett. B* **673**, 192 (2009).
- [118] V. Koch, A. Majumder, and J. Randrup, *Phys. Rev. Lett.* **95**, 182301 (2005).
- [119] B.-J. Schaefer and J. Wambach, *Phys. Part. Nucl.* **39**, 1025 (2008).
- [120] M. Wagner, A. Walther, and B.-J. Schaefer, *Comput. Phys. Commun.* **181**, 756 (2010).